In-situ observations of the isotopic composition of methane at the Cabauw tall tower site

Thomas Röckmann[1,*], Simon Eyer[2,*], Carina van der Veen[1], Maria E. Popa[1], Béla Tuzson[2], Guillaume Monteil[1,3], Sander Houweling[1], Eliza Harris[2], Dominik Brunner[2], Hubertus Fischer[7], Giulia Zazzeri[4], David Lowry[4], Euan G. Nisbet[4], Willi A. Brand[5], Jaroslav M. Necki[6], Lukas Emmenegger[2] and Joachim Mohn[2]

[1] Utrecht University (UU), Institute for Marine and Atmospheric Research Utrecht (IMAU), The Netherlands

[2] Empa, Laboratory for Air Pollution / Environmental Technology, Dübendorf, Switzerland

[3] now at Department of Physical Geography and Ecosystem Science, Lund University, Lund, Sweden

[4] Royal Holloway University of London (RHUL), Department of Earth Sciences, Egham, UK

[5] Max-Planck-Institute (MPI) for Biogeochemistry, Jena, Germany

[6] Environmental Physics Group, Faculty of Physics and Applied Computer Science, AGH University of Science and Technology, Krakow, Poland

[7] University of Bern, Climate and Environmental Physics, Bern, Switzerland

*These authors contributed equally to this work

Abstract

High precision analyses of the isotopic composition of methane in ambient air can potentially be used to discriminate between different source categories. Due to the complexity of isotope ratio measurements, such analyses have generally been performed in the laboratory on air samples collected in the field. This poses a limitation on the temporal resolution at which the isotopic composition can be monitored with reasonable logistical effort. Here we present the performance of a dual isotope ratio mass spectrometric system (IRMS) and a quantum cascade laser absorption spectroscopy (QCLAS) based technique for in-situ analysis of the isotopic composition of methane under field conditions. Both systems were deployed at the Cabauw experimental site for atmospheric research (CESAR) in the Netherlands and performed in-situ, high-frequency (approx. hourly) measurements for a period of more than 5 months. The IRMS and QCLAS instruments were in excellent agreement with a slight systematic offset of (+0.25 ± 0.04) ‰ for $\delta^{13}C$ and (-4.3 ± 0.4) ‰ for δD. This was corrected for, yielding a combined dataset with more than 2500 measurements of both $\delta^{13}C$ and δD. The high precision and temporal resolution dataset does not only reveal the overwhelming contribution of isotopically depleted agricultural CH_4 emissions from ruminants at the Cabauw site, but also allows the identification of specific events with elevated contributions from more enriched sources such as natural gas and landfills. The final dataset was compared to model calculations using the global model TM5 and the mesoscale model FLEXPART-COSMO. The results of both models agree better with the measurements when the TNO-MACC emission inventory is used in the models than when the EDGAR inventory is used. This suggests that high-resolution isotope measurements have the potential to further constrain the methane budget, when they are performed at multiple sites that are representative for the entire European domain.

1. Introduction

The global increase of the important greenhouse gas methane in the atmosphere since the beginning of the industrial period is very well established (Dlugokencky et al., 2009; Dlugokencky et al., 1996; Dlugokencky et al., 1998; Etheridge et al., 1998; Khalil et al., 2007; Loulergue et al., 2008; MacFarling Meure et al., 2006; Rasmussen and Khalil, 1981; Spahni et al., 2005). The existing CH_4 mole fraction measurement data enable accurate assessment of the source-sink imbalance through time, and together with the estimated total sink strength, they allow for a top-down constraint on the global source of methane to the atmosphere (Bergamaschi et al., 2013; Houweling et al., 2014). Bottom-up estimates of the global methane budget carry much larger uncertainties, which are inherent to the assumptions made in the extrapolation of local scale measurements to larger scales (Bruhwiler et al., 2014; Kirschke et al., 2013; Nisbet et al., 2014). The advantage of bottom-up estimates is, however, the possibility to distinguish different sources and to link observations to process-level understanding of the emissions.

An independent approach for distinguishing between source categories of CH_4 is the analysis of its isotopic composition, which is strongly linked to the source/sink processes. This is particularly true for methane from biogenic, thermogenic and pyrogenic sources (Gros et al., 2004; Houweling et al., 2008; Quay et al., 1999; Sapart et al., 2012). A more detailed differentiation within one source category, e.g. biogenic CH_4, for emissions from wetlands, ruminants, rice paddies or termites, however, is complicated because of the overlap of the respective isotopic source signatures. Further complications arise because individual source signatures can show pronounced dependence on environmental parameters and metabolized substrates (Kawagucci et al., 2014; Klevenhusen et al., 2010). In addition to the source contributions, the sink processes (mainly chemical removal by the hydroxyl radical (OH), but also soil deposition and stratospheric loss) also affect the isotopic composition of atmospheric methane (Brenninkmeijer et al., 1995; Röckmann et al., 2011; Saueressig et al., 1996; Saueressig et al., 2001; Snover and Quay, 2000). Nevertheless, over the past decades, numerous studies have shown the potential of isotope measurements to identify individual source categories from isotope

observations (Beck et al., 2012; Lassey et al., 1993; Tarasova et al., 2006; Umezawa et al., 2012b; Zazzeri et al., 2015) and to constrain budgets (Ferretti et al., 2005; Fischer et al., 2008; Houweling et al., 2008; Lassey et al., 2000; Lowe et al., 1994; Sapart et al., 2012; Umezawa et al., 2012a).

The isotopic composition is commonly reported in δ notation, where δ quantifies the relative deviation of an isotope ratio (^{13}R = $^{13}C/^{12}C$ for carbon isotopes and ^{2}R = $^{2}H/^{1}H$, abbreviated as D/H, for hydrogen isotopes) in a sample from a standard ratio. The international standard for reporting $\delta(^{13}C, CH_4)$ values is Vienna Pee Dee Belemnite (VPDB, $^{13}R_{VPDB}$ = 0.0112372 (Craig, 1957)) and for $\delta(D, CH_4)$ it is Vienna Standard Mean Ocean Water (VSMOW, $^{2}R_{VSMOW}$ = 0.0020052 (Baertschi, 1976)). $\delta(^{13}C, CH_4)$ and $\delta(D, CH_4)$ are abbreviated as $\delta^{13}C$ and δD in the following, and given in per mill (‰). CH_4 mole fractions $\chi(CH_4)$ are reported in nmol/mol = 10^{-9} and μmol/mol = 10^{-6}. For interpretation of global or continental scale atmospheric data the expert group of the WMO/IAEA has set a scientifically desirable level of compatibility of 2 nmol/mol, 0.02 ‰ and 1 ‰ for CH_4 fraction, $\delta^{13}C$ and δD, respectively (WMO, 2014). For regionally focused studies with large local fluxes, extended compatibility goals of 5 nmol/mol, 0.2 ‰ and 5 ‰ for $\chi(CH_4)$, $\delta^{13}C$ and δD were defined.

Due to the complexity of the involved measurement techniques, CH_4 isotope measurements have been limited mostly to relatively low frequency sampling in the field followed by isotope analysis in the laboratory (Bock et al., 2010; Brass and Röckmann, 2010; Sapart et al., 2011; Sperlich et al., 2013; Umezawa et al., 2009; Yamada et al., 2003). For many decades, the dominant method for high precision isotope analysis of atmospheric methane was isotope ratio mass spectrometry. In particular, the development of continuous-flow IRMS in the past two decades (Merritt et al., 1994; Merritt et al., 1995) has greatly increased the throughput of IRMS methods, making this the technique of choice in most laboratories, also because of the small sample amounts required.

Recently, mid-infrared laser absorption spectroscopy has proven its potential for high precision isotope ratio analysis. First attempts of measuring the isotopic composition of methane (Bergamaschi et al., 1998a; 1998b; 1994) were restricted to enhanced CH_4 fractions (>50 μmol/mol for $\delta^{13}C$ and >2000

μmol/mol for δD) and required cryogenic cooling for both the laser source and the detector, which impeded in-situ and long-term applications. The invention of room temperature, quantum cascade laser (QCL) sources has triggered the development of a novel generation of spectrometers suitable for in-situ analysis of the isotopic composition of greenhouse gases (Eyer and al, 2015; Tuzson et al., 2008; Wächter et al., 2008). Their capability of high-temporal resolution led to new applications aiming for source attribution (Mohn et al., 2012; Tuzson et al., 2011; Wolf et al., 2015). The advantages of in-situ measurements are particularly apparent in combination with atmospheric modeling techniques, which enables the identification of specific source regions (Rigby et al., 2012; Sturm et al., 2013). Similarly, high-frequency, high-precision CH_4 isotope data are expected to greatly reduce uncertainties of national and global source estimations, as demonstrated in an observing system simulation experiment (Rigby et al., 2012).

In this paper we present the analytical setup and results of a 5-month campaign at the Cabauw tall tower site in the Netherlands, where the isotopic composition ($\delta^{13}C$ and δD) of CH_4 was measured with two instruments, one IRMS system developed at Utrecht University and one QCLAS-instrument developed at Empa. The compatibility of the two analytical techniques for CH_4 mole fractions, $\delta^{13}C$-CH_4 and δD-CH_4 is assessed and the obtained high-resolution isotope dataset is exploited using a novel moving Keeling plot method. A comparison of measurement results with calculations from two different models (TM5 and FLEXPART-COSMO) and two emission inventories (EDGAR, TNO-MACC) indicates the potential of this approach to better constrain on isotope source signatures and emissions in atmospheric models.

2. Methods

2.1. Site description

The 213 m tall tower is the central construction of the Cabauw Experimental Site for Atmospheric Research (CESAR, http://www.cesar-observatory.nl/, 51° 58’ N, 4° 55’ E, 2 m a.s.l.). The CESAR site is dedicated to atmospheric research and hosts a wide variety of instruments for in situ and remote sensing measurements of meteorological parameters, trace gases, pollutants, aerosols, and clouds. The

site is located in an agricultural landscape, with CH_4 emissions originating from ruminants and other agricultural activities, but also from the peaty soil and the drainage ditches between the surrounding fields (Peltola et al., 2014). The small town Lopik (~7500 inhabitants) is located 1 km east of the tower. Population and road density increase steeply further away from the tower towards the country's major cities: Utrecht (at about 20 km distance), Rotterdam (30 km), the Hague (40 km) and Amsterdam (45 km). An estimated seven million people inhabit these cities and their many neighboring settlements. The location and surroundings are described in more detail in (Peltola et al., 2014; Peltola et al., 2015; Vermeulen et al., 2011). The instruments were operated in a room on the ground floor of the CESAR building. Since this room is not commonly used as laboratory, it has air-conditioning with limited cooling capacity and the temperature varied between 25 ˚C and 30 ˚C.

2.2. Air sampling at the Cabauw tall tower

Air was continuously drawn through ½" o.d. (outer diameter) Dekabon tubing from 20 m height at a total flow of 16 l min^{-1} provided by a Varian scroll pump (Agilent Technologies Inc., USA). The sample gas flow was adjusted by means of a flow restriction at the inlet of the pump in order to maintain the pressure in the sampling line above 950 hPa. The sample gas flows for the methane isotope analyzers were branched off upstream of the scroll pump and the restriction, using ¼" o.d. Dekabon lines.

2.3. IRMS system

The new IRMS method for $\delta^{13}C$ and δD analysis of atmospheric CH_4 is based on the ISAAC system as developed at the MPI for Biogeochemistry in Jena (W. Brand et al., manucript in preparation). Importantly, the system does not require liquid nitrogen coolant for the preconcentration and focusing steps, but uses a massive copper block cooled down to about -145 ˚C, to which the cold traps for preconcentration and cryo-focussing are connected via standoffs (see 2.3.1). This cold assembly is contained in an evacuated steel Dewar to prevent condensation of moisture. During the campaign, the extraction unit and two IRMS instruments (Thermo Delta Plus XL for hydrogen isotopes and Thermo Delta Plus XP for

carbon isotopes, both Thermo Fisher Scientific Inc., Germany) were operated at the CESAR site. The system is schematically shown in Fig. 1.

2.3.1. Cryogenic trapping

A Polycold compact cooler compressor (Brooks Automation Inc., USA), filled with coolant PT-30, cooled a cold end on which a copper cylinder (70 mm diameter, 85 mm height, 3 kg) was mounted. In this configuration, the copper block reached a temperature of -145 ˚C. The pre-concentration trap (PreCon) was a 10 cm 1/8" SS tube filled with 4 cm 60/80 mesh HayeSep D in the center and 3 cm 60/80 glass beads on each end. It was connected with Valco fittings and the packing material was retained in the trap using removable frits (CEF1F, Valco Instruments Company Inc., USA). The focus trap (Focus) was a 10 cm 1/16" SS tube filled with 2 cm HayeSep D and 4 cm glass beads at both ends, connected with Valco fittings (ECEF211.0F, Valco Instruments Company Inc., USA). The traps could be heated with 0.5 m Thermsys heating wire wrapped around the tubes. The PreCon and Focus trapping units were glued together with a PT-100 temperature sensor in heat‐conducting two component epoxy on a brass standoff. These brass standoffs were mounted to the copper cylinder. In the "trapping" configuration the temperatures of the traps were usually kept at -135 ˚C.

2.3.2. Measurement procedure

A 3-port 2-position Valco valve (3PV, Fig. 1) selected either ambient air drawn from the tower through a $Mg(ClO_4)_2$ dryer, or cylinder air that was injected via one port of an 8-port multiposition Valco valve (MPV). To check the system performance, a reference air cylinder (Ref) was measured alternately with ambient air, and three other target gas cylinders were measured occasionally. The inlet line was connected to a 4-port 2-position Valco valve (4PV1), which directed either Helium (He, BIP quality, Air Products and Chemicals Inc., USA) or the selected airflow to the PreCon unit, which was connected in the loop position of a 6-port 2-position Valco valve (6PV). All He and air flows were controlled by MKS mass flow controllers (MFC, MKS Instruments Inc., USA).

The preconcentration and cryofocussing was done similarly to Brass and

Röckmann (2010). After flushing the inlet line with >20 ml air, the 6PV was switched to the load position and air was admitted to the PreCon unit. The duration of the air sampling for the IRMS system was 10 minutes at a flow rate of 5 ml min^{-1} for $\delta^{13}C$ and 7 ml min^{-1} for δD. The flow was provided by a Xavitech mini pump (P200-GAS-12V, Xavitech AB, Sweden). During this step, the temperature measured at the PreCon stayed below -132 ˚C. At this temperature CH_4 and several other trace species were retained on the HayeSep D, while the air matrix was efficiently flushed out.

After preconcentration, the PreCon unit was heated to -30 ˚C and a He flow of 3 ml min^{-1} transported the CH_4 in 90 seconds to the Focus unit, which was held at a temperature <-137 ˚C. After transfer of the sample to the Focus, the 6PV was switched to the load position and the PreCon was heated to -10 ˚C to release any remaining trapped gases such as CO_2.

The Focus was then heated to release the CH_4, which was directed via 4PV2 and 4VP3 either to the combustion oven and the Delta plus XP IRMS for ^{13}C analysis or to the pyrolysis oven and the Delta plus XL IRMS for D analysis.

For δD analysis, the CH_4 was injected into a pyrolysis tube furnace (1400 ˚C), where CH_4 was converted to H_2 and carbon. The H_2 entered the IRMS, after passing a 2 m CarboPLOT column at room temperature (RT) and a nafion dryer, via the GasBench interface. No krypton interference (Schmitt et al., 2013) could be determined in this setup. The repeatability for δD was generally better than ±2 ‰ (reported as SD), based on consecutive analyses of reference air.

For $\delta^{13}C$, the CH_4 was injected from the cryofocus unit into a combustion oven containing a nickel / nickel oxide wire catalyst at 1100 ˚C, where the CH_4 was converted to CO_2 and H_2O. The resulting gas mixture passed a nafion dryer and a 10 m PoraPLOT Q column (5 ˚C) to eliminate interference from co-trapped krypton (Schmitt et al., 2013) before entering the IRMS via the GasBench interface. The repeatability of $\delta^{13}C$ was better than ±0.07 ‰ (reported as SD), based on consecutive analyses of reference air.

The typical measurement order during the Cabauw campaign was Ref $\delta^{13}C$ – Air $\delta^{13}C$ –Ref δD – Air δD. A full measurement cycle took 84 min. On a regular basis, pressurized air from a cylinder, applied as a target gas, was analyzed as a quality

control tool in order to monitor the long term stability of the analytical technique. The CH_4 mole fraction and isotopic composition in ambient air and target gas were calculated using an interpolation of the reference air analyzed before and afterwards. A custom made LabView software program (National Instruments Corp., USA) was used to control and log the temperature of the traps, the valve switching and the flow setpoints of the MFCs.

2.3.3. IRMS system isotope calibration

The isotope calibration of the IRMS system was based on a reference air cylinder that contains ambient air collected at the IMAU in 2014, with 1888 nmol/mol of CH_4 and isotope values of $\delta^{13}C$ = -47.89 ‰ and δD = -88.08 ‰. The isotope calibration scale is based on the reference scale that was described in detail in Brass and Röckmann (2010). We used the average of the reference air measurement before and after the sample air measurement to calculate the mole fraction and δ values. The linear response of the analytical system (independence of the δ value on the amount of CH_4 analyzed) was verified by injecting various volumes of reference air up to a volume equivalent to 2700 nmol/mol. Occasionally, the long-term stability of the system was checked by measuring 3 target cylinders with different CH_4 mole fractions and isotopic compositions. A robust link of the isotopic composition to the international reference materials VPDB and VSMOW has been established in the framework of the INGOS project (Sperlich et al., 2016).

2.4. QCLAS system

The analytical procedure of the laser based measurement system involves two steps: preconcentration of the CH_4 from 7.5 L of ambient air in a trace gas extractor (TREX) by adsorption on HayeSep D (Eyer et al., 2014; Mohn et al., 2010) and analysis of CH_4 isotopologues with a modified commercial QCLAS (QCL-76-D, Aerodyne Inc., USA). Details on the development, optimization and validation of the TREX-QCLAS system are given by Eyer et al. (2015).

The present manuscript comprises the first application of the TREX-QCLAS system for in-situ analysis of CH_4 isotopologues at a field site for an extended period of time. In comparison to the original setup, the heating power of the

polyimide foil on the cold trap was reduced to 60 W to increase its lifetime. Due to the lower heating power, the duration of the desorption step had to be extended, which led to an improved separation from residual bulk gases (e.g. N_2 and O_2). Lowering the O_2 enhancement in the gas matrix is also the main reason for a lower offset in $\delta^{13}C$ of 1.58 ‰, with respect to the MPI - scale, as compared to 2.3 ‰ in previously published results (Eyer et al., 2015). The offset was related to a higher O_2 mole fraction in the gas matrix after CH_4 preconcentration. One measurement cycle consisted of four consecutive measurements of ambient air samples and one sample of pressurized air used as a target gas, followed by a calibration phase and took around 4:30 hours. This translates into an analysis time of 54 minutes per sample of ambient or pressurized air.

A calibration gas (CG1, (1200 ± 50) µmol/mol CH_4, $\delta^{13}C$ = -(44.24 ± 0.10) ‰, δD = -(104.7 ± 1.1) ‰) was diluted to 688 µmol/mol and analyzed between every preconcentrated sample as an anchor to correct the measurements for instrumental drift. A second calibration gas (CG2, (1103.8 ± 3.5) µmol/mol CH_4, $\delta^{13}C$ = -(36.13 ± 0.10) ‰, δD = -(180.6 ± 1.1) ‰), diluted to a similar CH_4 mole fraction of 681 µmol/mol was used to calculate calibration factors for $\delta^{13}C$ and δD values. Furthermore, gas cylinders of pressurized ambient air, referred to as target gas (TG1, TG2), were frequently measured over the entire campaign to determine and verify the repeatability of the measurement system, which was found to be 0.28 ‰ and 1.7 ‰ for $\delta^{13}C$ and δD (1σ), respectively. Additional adjustments in the preconcentration procedure and in the analytical routine for isotope analysis improved the repeatability to 0.18 ‰ and 0.85 ‰ for $\delta^{13}C$ and δD in the last month of the campaign. One example is the improved temperature control of the trap during adsorption, which in turn stabilized the O_2 content in the measuring gas and thereby reduced variations in $\delta^{13}C$-CH_4.

The CH_4 isotopic composition of the calibration gases, as well as the target gases (TG1, (2639.5 ± 0.6) nmol/mol CH_4, $\delta^{13}C$ = -(46.48 ± 0.10) ‰, δD = -(119.0 ± 1.1) ‰, TG2, (2659.8 ± 0.6) nmol/mol CH_4, $\delta^{13}C$ = -(45.87 ± 0.10) ‰, δD = -(114.1 ± 1.1) ‰) were determined by the Stable Isotope Laboratory at the Max-Planck-Institute for Biogeochemistry. CH_4 mole fraction measurements were linked to

the WMO-X2004 calibration scale (Dlugokencky et al., 2005) through calibration of the target gases against NOAA reference standards at Empa.

2.5. Modeling

Two complementary atmospheric transport models (TM5, FLEXPART-COSMO), both in combination with two different emissions inventories (TNO-MACC_2, EDGAR/LPJ-WhyMe), were applied to support interpretation of the measurements. The Eularian tracer model TM5 simulated the distribution of CH_4 and $^{13}CH_4$ at global scale with a zoom on Europe at 1° x 1° resolution and considered both the isotopic signatures of different sources and the fractionation by different removal pathways of CH_4 in the atmosphere. The Lagrangian particle dispersion model FLEXPART-COSMO, conversely, was run in backward mode at a higher resolution of 0.06° x 0.06° but only over Europe. This model is better able to represent the spatial variability of CH_4 sources in the near field of Cabauw but it only simulated the contributions from the last 4 days of emissions within Europe and not the large-scale background. Chemical loss of CH_4 was not considered due to the short transport times between the sources and the receptor point at Cabauw. δD was only simulated with FLEXPART-COSMO.

2.5.1. TM5 modeling

Simulations of atmospheric CH_4 and $\delta^{13}C$ were performed using the global tracer model TM5 (Krol et al., 2005). The Eularian off-line model was driven by meteorological fields from the European Centre for Medium Range Weather Forecast (ECMWF) reanalysis project ERA-Interim (Dee et al., 2011), pre-processed for use in TM5. For vertical transport due to moist convection we made use of Era Interim archived convective mass fluxes, replacing the use of the Tiedke scheme in Krol et al. (2005). The model was run at a horizontal resolution of 6^ox4^o globally and 1^ox1^o inside a zoom domain covering Western Europe. The model uses 25 hybrid sigma-pressure levels from the surface to top of atmosphere.

Two parallel (forward) TM5 simulations were performed with CH_4 and $^{13}CH_4$ as transported tracers. In the standard configuration, anthropogenic CH_4 emissions were taken from EDGAR4.2 FT2010 (EDGAR, 2009), extrapolated to 2014 and

2015 using annual statistics from the Food and Agriculture Organization of the United Nations (FAO) and the British Petroleum Company (BP), as described in Houweling et al. (2014). For natural wetland emissions, an average of the emission estimates derived by Spahni et al. (2011) for the period 2003-2008 was taken, using the LPJ-WhyMe model. For a complete description of the CH_4 emissions (Table 1), see Monteil et al. (2013) and references therein. $^{13}CH_4$ emissions were derived from the CH_4 emissions using prescribed $\delta^{13}C$ source signatures (Table 1). The emission inventory was built according to a double constraint: 1st, each source signature must be chosen within its own uncertainty interval, and 2nd, the resulting global average source signature must be compatible with the global source signature that is inferred from the observations (and that is known with a much better precision than the individual source signatures) (Monteil et al., 2011). In a second set of simulations, anthropogenic emissions in a regional domain centered on Cabauw were replaced by emissions from the European TNO-MACC_2 inventory, which was used as the standard inventory in the FLEXPART-COSMO simulations (see below). Outside the regional domain covered by TNO-MACC_2, the EDGAR emissions were used.

Atmospheric removal of CH_4 was modeled as described in Monteil et al. (2013), using kinetic fractionation factors $\alpha = k(^{12}C) / k(^{13}C)$ of $\alpha_{OH} = 1.0055$, $\alpha_{Cl} = 1.066$ and $\alpha_{O(1D)} = 1.013$ for the reactions between CH_4 and OH (Sander et al., 2006), Cl (Saueressig et al., 1995) and $O(^1D)$ (Saueressig et al., 2000), respectively. The simulations were initialized at steady state (obtained via a spin-up run) in 2005, and simulations of the period 2005-2015 were used to calculate a realistic state of the atmosphere at the start of the measurement campaigns, including the imbalance between emissions and atmospheric CH_4 mixing ratio/isotopic composition in 2014. Time series were extracted from model-simulated mole fraction fields after interpolation to the horizontal coordinate and height of the Cabauw tower air inlet.

2.5.2. FLEXPART-COSMO modeling

The Lagrangian Particle Dispersion Model (LPDM) FLEXPART (Stohl et al., 2005) was used in a modified version coupled to the mesoscale numerical weather

forecast model COSMO (Baldauf et al., 2011) to simulate the regional contribution of different source categories to the concentrations and isotopic signatures of CH_4 at Cabauw. FLEXPART–COSMO was driven by hourly operational analysis fields generated by the Swiss national weather service MeteoSwiss for a domain covering entire western and central Europe from Ireland, Denmark, and Poland in the north to Portugal and southern Italy in the south with a horizontal resolution of approximately 7 km x 7 km and 60 vertical levels. Every 3 hours, 50'000 particles (air parcels) were released from the position of the inlet 20 m above surface and traced backward in time for 4 days to compute the sensitivity of each 3-hourly measurement to upwind sources. The corresponding source sensitivity maps or footprints (Seibert and Frank, 2004) were multiplied with gridded CH_4 emissions to compute the mole fraction enhancement above background expected from different sources. Emissions were taken from the TNO-MACC_2 inventory for Europe representative of the year 2009 and available at 0.125° x 0.0625° resolution (Kuenen et al., 2014) or, alternatively, from the same version of EDGAR/LPJ-WhyMe inventory driving TM5 at a resolution of 1° x 1°. Methane mole fractions were computed separately for a number of SNAP (Standardized Nomenclature for Air Pollutants) source categories with specific isotopic signatures as summarized in Table 2.

For the domain covered by the FLEXPART-COSMO simulations, which includes most of western and central Europe, total anthropogenic emissions are 20.6 Tg CH_4/yr in EDGAR and 18.3 Tg CH_4/yr in TNO-MACC, which corresponds to a difference of 12.5%. CH_4 emissions from gas/oil production and distribution are 89% higher, CH_4 emissions from agriculture 19% lower and CH_4 emissions from waste 12% higher in EDGAR than in TNO-MACC.

Source specific emissions were combined with isotopic signatures of the various categories from Table 2 to derive mean $\delta^{13}C$ and δD isotopic signatures for the CH_4 that was picked up by the air parcel along the trajectory.

2.6. Interpretation of CH_4 isotope data

2.6.1. Data analysis by a Keeling plot technique

The isotopic composition of CH_4 emissions were estimated using the Keeling plot technique (Keeling, 1961; Pataki et al., 2003). This method allows the isotopic signature of a single source process or the mean isotopic signature of combined source processes that mix into a background reservoir to be determined from the observed ambient isotopic composition and mole fraction. An implicit assumption of the Keeling plot approach is that the isotopic composition and mole fraction of the background reservoir and the isotopic composition of the source or the combined source stay constant over the time range of the analysis. This may not always apply as the relative contribution of individual CH_4 sources or their isotopic signature may change over time

To exploit the high temporal resolution of our data, we applied a novel approach of a moving Keeling plot (MKP) method. Data within a moving window of 12 hours were used to calculate the source isotopic composition. This window was moved in 1-hour time steps over the data series. In addition, values for background conditions within a 48-hour period, centered on the respective 12-hour window, were included in the analysis. These background values were chosen between 10:00 and 18:00 local time, because during this period a convective boundary layer usually develops and hence local influence is weak; pollution events with CH_4 mole fractions above 2100 nmol/mol were filtered out additionally. For each time window, an orthogonal least squares fit was applied to the δ values vs. the inverse CH_4 mole fractions and R^2 values were calculated. A Keeling plot analysis only returns meaningful values for the source isotopic composition if the variations in CH_4 mole fraction are significant and if the emissions are from a source with a well-defined isotopic composition. Therefore, two additional filters were applied: i) the mole fraction had to vary by more than 200 nmol/mol within each time window and ii) the R^2 of the fit had to be larger than 0.8. If $R^2 < 0.8$, the 12 h interval was reduced consecutively by one hour to a minimum of six hours until either the R^2 of the fit was > 0.8 or the number of data points was lower than five. On average this technique accumulated 22 data points per 12-h time window.

3. Results

3.1. Overview of the field measurements at the Cabauw site

The full record of the methane mole fraction and isotopic composition obtained with the two measurement techniques at the CESAR site is shown in Fig. 2. The IRMS system started with δD measurements first, and after 3 weeks delivered both $\delta^{13}C$ and δD data. The TREX-QCLAS system started later and ran continuously from mid-December to mid-January, and from mid-February to the end of the campaign. Despite a number of interruptions mainly due to various kinds of instrument malfunction, the combined time series of both techniques shows a high temporal coverage with more than 2500 measurements performed for both $\delta^{13}C$ and δD.

A qualitative inspection of the time series already conveys the obvious features that will be discussed below in more detail: the methane mole fraction $\chi(CH_4)$ shows a large number of substantial increases above background level, and these positive methane excursions are accompanied by negative excursions in the δ values from the background level. Thus the additional methane is generally depleted in both ^{13}C and D.

3.2. Inter-comparison of the two analytical techniques

Before presenting a detailed analysis of the CH_4 isotopic composition in ambient air, we compare the results obtained with the IRMS and QCLAS techniques in order to evaluate their performance and to combine the results into one final dataset. Although both systems measured air from the same intake line, the sampling intervals could not be synchronized since both instruments operated in different measurement cycles. A full measurement cycle (including measurement of the reference gas) took 84 minutes for the IRMS system and 54 minutes for the TREX-QCLAS system. The actual duration of the air sampling was 10 minutes for the IRMS system and 15 minutes for the QCLAS system. So even if the systems coincidentally started sampling at the same time, they never actually analyzed exactly the same air mass. Consequently, differences between the systems contain contributions from natural variability, random fluctuations due to limited measurement precision, and system offsets.

Fig. 2 shows a comparison of the $\chi(CH_4)$, as well as $\delta^{13}C$ and δD values that were obtained with the TREX-QCLAS and the IRMS technique. To visualize the possible effect of time shifts, the size of the points corresponds to the proximity of the

sampling intervals. A total of 727, 333 and 277 measurement pairs for $\chi(CH_4)$, $\delta^{13}C$ and δD, respectively, analyzed by both techniques were combined in this way.

The mole fraction comparison shows good agreement along the 1:1 line but with a large scatter, which has two contributions: i) instrumental noise, as the isotope systems have a relatively large uncertainty for measurement of the mole fraction compared to existing high-precision CH_4 analyzers, and ii) natural variability associated with the sampling of different air masses as described above. The second point is supported by the fact that the average difference in CH_4 mole fractions between the two analytical techniques was larger for larger temporal differences in the sampling intervals.

For the isotope intercalibration plots, the grey-black shading of the circles indicates the difference in $\chi(CH_4)$ of the respective measurement pair analyzed by both techniques. The overall difference between the measurements conducted with the two systems (QCLAS-IRMS) is (+0.25 ± 0.04) ‰ for $\delta^{13}C$ and (-4.3 ± 0.4) ‰ for δD (the stated errors are standard errors of the mean). The mean offsets are slightly outside the WMO extended compatibility goals for $\delta^{13}C$ (0.2 ‰) and within the WMO extended compatibility goals for δD (5 ‰), as indicated by the red dashed lines (WMO, 2014). Individual measurement pairs can show significantly larger deviations for aforementioned reasons. Differences between the two techniques are higher than expected as both laboratories refer their measurements to MPI-BGC, who recently established a link between the CH_4 isotopic composition and the international reference materials VPDB and VSMOW, in the framework of the INGOS project (Sperlich et al., 2016). Therefore, remaining differences can only be rationalized by uncertainties in propagating the scale or by instrumental issues. The enhanced discrepancies for low δD-CH_4 values might originate from a non-linear response of one of the applied analytical techniques. The mean offset values determined above were applied to the QCLAS data to create one combined dataset with 2610 data points for $\delta^{13}C$ and 2673 data points for δD.

3.3. FLEXPART-COSMO source attribution

In FLEXPART-COSMO, the contributions of the individual source types are simulated separately and added up to obtain the cumulative CH_4 mole fraction. Fig. 4 shows these contributions in absolute (top) and relative terms (bottom). According to the model, the relative contributions at the Cabauw site are quite uniform, with agricultural sources accounting for more than 60%, waste (mostly landfills) around 20–40%, and fossil sources between 0 and 40%. We note that significant contributions from fossil sources are only detected episodically, during several events that usually last a few days. Contributions from other source categories are generally negligible at the Cabauw site.

3.4. TM5 and FLEXPART-COSMO modeling including isotopes

The TM5 model calculates the combined influence of the global methane sources and sinks on CH_4 and $\delta^{13}C$ at the Cabauw tower, and therefore the TM5 results can be compared directly to the measured time series. For FLEXPART-COSMO, a representative background mole fraction and isotopic signature needs to be added for comparison with the observations. For simplicity we assumed a constant background similar to the observed values for background conditions: 1930 nmol/mol for $\chi(CH_4)$ with $\delta^{13}C$ = -47.1 ‰ and δD = -86 ‰.

Fig. 5 shows a comparison of these model-generated time series with the measured data for the entire campaign. Both models capture the amplitude and the temporal variability of $\chi(CH_4)$well. Most of the methane pollution events observed at the CESAR site are also present in the modeled time series and the increase in $\chi(CH_4)$ is of a comparable size. In addition, the results of the TM5 and the FLEXPART-COSMO model for CH_4 mole fractions agree relatively well with each other (R^2=0.69), in particular when both models are run with the same inventory at the same coarse spatial resolution, i.e. with EDGAR/LPJ-WhyMe.

A few pronounced CH_4 events in Fig. 5 show larger differences between the models. On 2 November, FLEXPART-COSMO simulates an emission signal that is not captured by TM5. Unfortunately no measurements are available for this event to decide on which model performs better. On 30 November TM5 simulates a CH_4 plume, which is absent in FLEXPART-COSMO, and this event is also not supported by the measurements. The global model has the advantage

523 that it includes the influence of long-range transport. As expected, however, the
524 observed variability is predominantly influenced by local and regional emissions.
525 Regarding the time series of the δ values, both TM5 and FLEXPART-COSMO
526 qualitatively display the expected anti-correlations between CH_4 and $\delta^{13}C$.
527 However, the amplitude of the $\delta^{13}C$ variability is generally underestimated in the
528 model runs, especially when using the EDGAR inventory. In addition, the
529 modeled background level of $\delta^{13}C$ in TM5 is offset by up to 1 ‰, but this offset is
530 also present at clean background sites in the Northern hemisphere.
531 Using the TNO-MACC inventory in FLEXPART-COSMO results in better
532 agreement with the observed variability of $\delta^{13}C$. In TM5, the TNO-MACC
533 emissions reduce the amplitude of the CH_4 variability, which is explained by the
534 13% lower emissions in TNO-MACC compared with EDGAR. Furthermore, the
535 results of both models are consistent with the emissions being more depleted in
536 $\delta^{13}C$ in TNO-MACC than in EDGAR. The measurements indicate emissions that
537 are even more depleted in $\delta^{13}C$ than TNO-MACC values. These results suggest
538 that the fractional contribution of isotopically heavy fossil emissions is
539 overestimated in EDGAR, at least in the area sampled by Cabauw, although the
540 uncertainty in the assumed $\delta^{13}C$ source signatures could also contribute. For
541 instance, recent literature showed that landfill emissions from the UK are more
542 depleted in $^{13}CH_4$ due to the implementation of gas extraction systems (Zazzeri
543 et al., 2015).
544 The δD time series simulated with FLEXPART-COSMO using the TNO-MACC
545 inventory is in good agreement with the measurements. This further indicates
546 that TNO-MACC has a realistic source mixture, but the uncertainties in the mean
547 δD signature are too large to draw firm conclusions at this stage. Despite these
548 uncertainties, Fig. 5 clearly demonstrates how isotopic measurements highlight
549 differences between emission inventories, which would go unnoticed looking
550 only at CH_4 mole fractions. Additional information may be available from the
551 combination of both isotope signatures. For several of the CH_4 elevation events
552 shown in Fig. 5b, the relative changes in $\delta^{13}C$ and δD modeled with FLEXPART-
553 COSMO vary when using the two different inventories (TNO-MACC and EDGAR).
554 Some of the anomalies show differences pointing in the same direction for $\delta^{13}C$

555 and δD, and some others not. This suggests that δD provides additional
556 independent information, which will be discussed in more detail in Section 4.3
557 using a double isotope plot of the source signatures (Fig. 7). The benefit of the
558 high-resolution dual isotope measurements for validating emissions used in the
559 models will be investigated in Section 4.4.

560 **4. Discussion**

561 **4.1. Diurnal and synoptic variability**

562 A prominent feature of the high-resolution dataset is the pronounced diurnal
563 variability, with large increases in CH_4 mole fraction that occur often during the
564 night, due to the shallow planetary boundary layer. In addition, there are also
565 several synoptic (but much smaller) pollution events, where CH_4 mole fractions
566 stay above the unpolluted background level for several days. These elevations
567 are likely caused by synoptic scale advection of CH_4 plumes from other source
568 regions with a different source mix.

569 **4.2. Isotope identification of the mean CH_4 source**

570 In Fig. 6, the Keeling plot technique is applied to identify the mean isotopic
571 signatures ($\delta^{13}C$, δD) of the combined CH_4 emissions detected at the Cabauw site.
572 An orthogonal regression method was applied to determine the fit parameters.
573 This analysis yields well-defined mean isotopic signatures of the cumulative
574 source (the y-intercept of the regression analysis) of $\delta^{13}C = -(60.8 \pm 0.2)$ ‰ and
575 $\delta D = -(298 \pm 1)$ ‰. The inferred mean isotopic signature agrees well with
576 emission from ruminants, which are expected to be the main source of CH_4 in
577 this rural area. This is plausible, because the mean isotopic signature is largely
578 determined by the pronounced nighttime CH_4 elevations, which represent the
579 local emissions close to the tower. Also the source contributions modeled by
580 FLEXPART-COSMO suggest the dominant influence of agricultural emissions in
581 this rural area (Fig. 4). Interestingly, the mean isotopic signature for the much
582 smaller synoptic CH_4 variations of the background (red points in Fig. 6) is not
583 significantly different from the one for the complete dataset.

584 **4.3. Short-term variability**

585 Given the high temporal resolution of the dataset presented here, the isotope
586 variations can be interpreted in much more detail than the overall analysis
587 performed above. This allows identifying varying contributions of CH_4 sources
588 during different periods of the campaign. To do so, we applied a 12-hour Moving
589 Keeling Plot (MKP) method to the data, as described in Sect 2.6.1.

590 Fig. 7 summarizes the results of the MKP method in the form of a δD vs. $\delta^{13}C$ plot.
591 To combine $\delta^{13}C$ and δD measurements performed at different times, MKP
592 intercepts were averaged over 6 h intervals. Mean $\delta^{13}C$ signatures range between
593 -68 ‰ and -55 ‰ and mean δD signatures cover a relatively wide range
594 between -350 ‰ and -260 ‰, indicating emissions mainly from microbial
595 sources as derived from the cumulative Keeling plot analysis. During some
596 periods, however, elevated mean $\delta^{13}C$ and δD signatures reveal significant
597 additional contributions from waste and/or fossil emissions.

598 The colored symbols in Fig. 7 highlight the mean isotopic signatures of three 48 h
599 events (10-12, 16-18 and 22-24 March) that are discussed in more detail in the
600 following. For the event of 16-18 March, selected results of the 12 h MKP method
601 are displayed in Fig. 7**,** demonstrating the advantage of the high temporal
602 resolution data. It is possible to clearly distinguish variations in the mean
603 isotopic signatures during this event by variations in the y-axis intercepts. The
604 increase by about 6 ‰ for $\delta^{13}C$ and about 50 ‰ for δD, in the source isotopic
605 signature for this event, clearly indicates the gradually increasing contribution of
606 CH_4 from isotopically enriched sources, e.g. fossil fuel- or waste-related CH_4.

607 The temporal evolution of the observed source mixture is investigated in further
608 detail in Fig. 9, where the 16-18 March period (labeled as 2) is compared to two
609 other 48 h – periods (10-12 March; label 1, and 22-24 March; label 3), each with
610 significant diurnal CH_4 elevations. For event 1, the mean isotopic signatures
611 stayed rather constant at values around $\delta^{13}C$ = -63 ‰ and δD = -320 ‰. These
612 values are typical for microbial emissions from an agricultural source and agree
613 well with the source contributions predicted for this period by the FLEXPART-
614 COSMO model.

615 Period 2 is characterized by much stronger isotopic change within the 48 h
616 period. The $\delta^{13}C$ signature increases to above -60 ‰ and the δD signature

increases to -240 ‰ by the end of the period (see Fig. 9). The double-isotope plot in Fig. 7 shows that the change in δD during event 2b clearly points towards fossil fuel sources, which provides independent support for the FLEXPART-COSMO simulations, where the contributions from fossil-fuel- derived emissions are higher for the second day.

For period 3, the mean $\delta^{13}C$ isotopic signatures increased during the 48 h by about 2-3 ‰, whereas the δD signatures remained constant around -300 ‰. For this period, the double isotope plot of Fig. 7 indeed shows a shift towards the waste category. Also this observation is independently confirmed (at least qualitatively) by the FLEXPART-COSMO model derived source attribution, which indicates the largest fraction of waste-derived CH_4 for the first day and a small addition of fossil CH_4 for the second day of event 3. These examples show that even at a location like Cabauw, where one source category strongly dominates, contributions from isotopically different sources can be identified if sufficiently high-resolution dual isotope ratio data are available. We note that the "directional" information in the double isotope plot is only available by combining $\delta^{13}C$ and δD measurements. It would be much harder, if not impossible, to detect an addition from fossil fuel- or landfill- derived CH_4 based on $\delta^{13}C$ or δD data alone.

4.4. Evaluation of emission databases with high temporal resolution CH_4 isotope data

As described in Section 3.4, both the TM5 and the FLEXPART-COSMO model-generated time series of CH_4 mole fractions show an adequate agreement with the CH_4 measurements at the Cabauw site. Therefore, the comparison between measurement data and the models can be used to evaluate the methane budget in more detail. In this context, the measured and modeled isotopic composition can be employed to assess the validity of emission inventories, EDGAR and TNO-MACC, with respect to the magnitude and spatial distribution of source categories. To compare the measured mean isotopic signatures to the model results, the simulated isotope time series were linearly interpolated and evaluated in the same way as the observations using the 12 h MKP method. This analysis was performed for both models (TM5 and FLEXPART-COSMO), each

using both the EDGAR/LPJ-Why-Me and the TNO_MACC inventories. Additionally, time series for the mean isotopic signatures were calculated directly from FLEXPART-COSMO data, without using of the MKP method. This direct method allowed an independent estimation of the mean isotopic signatures and, thus, also provided an opportunity to evaluate the MKP method.

The statistics of the mean isotopic signatures from all four model-inventory combinations are shown as histograms in Fig. 10**,** together with the measurement-derived mean isotopic signatures and the directly derived signatures from FLEXPART-COSMO modeling. A clear difference can be observed between the mean isotopic signatures derived with the two different emission inventories. Model runs with the EDGAR/LPJ-WhyMe emission inventory (red in Fig. 10) tend to produce mean CH_4 isotopic signatures that are more enriched in ^{13}C and D than the model runs with TNO-MACC emissions. These differences are very similar for the simulations using TM5 and FLEXPART-COSMO, suggesting that differences originate from the emission inventories, rather than from differences between the models themselves. The $\delta^{13}C$ source signatures derived from the measurements at the Cabauw tower are significantly more depleted than any of the model-generated datasets. For δD, the mean isotopic signatures using TNO-MACC emissions are relatively close to the measurements at Cabauw, whereas the values using EDGAR emissions are much more enriched in CH_3D.

The high temporal resolution isotope data that are described in this paper thus provide relevant information to further constrain models and/or emission inventories, because the mean isotopic signatures can change rapidly. The comparison of our first high-resolution isotope measurements at Cabauw to model calculations clearly identify differences between the modeled inventories, where the EDGAR inventory produced too enriched mean isotopic signatures due to a higher contribution from fossil fuel sources. Similar differences in terms of source contributions between EDGAR and TNO-MACC_2 were also reported by Hiller et al. (2014) for Switzerland, and Henne et al. (2015) concluded that natural gas emissions in Switzerland are likely overestimated in EDGAR.

5. Conclusions and outlook

The dual isotopic composition of CH_4 has been monitored for the first time with high temporal resolution in an extended (5 months) field deployment with two different instruments, an IRMS system and a QCLAS system, at the tall tower site Cabauw, the Netherlands. The measurements of both instruments compare well and can be combined to a time series of more than 2500 measurements for both $\delta^{13}C$ and δD. Using a moving Keeling plot technique, the mean isotopic signatures of periods with significant CH_4 elevations can be derived with high temporal resolution. The combination of $\delta^{13}C$ and δD data provides strong constraints to distinguish emissions from different source categories. Overall, CH_4 emissions at the Cabauw tall tower are dominated by agricultural sources, but variations in the mean isotopic signatures allow identification of events with increased contributions from fossil fuel and waste sources, which can be used to validate variations in the source mix, calculated using the FLEXPART-COSMO model.

The high-resolution isotope ratio measurements at Cabauw were compared to model calculations that used two different emission inventories. When two very different models (TM5 and FLEXPART-COSMO) used emissions from the EDGAR inventory, they produced clearly too enriched mean isotopic signatures. The modeled mean isotopic signatures were systematically more depleted and closer to the measured ones when the TNO-MACC inventory was used. The differences in the source signatures appear to originate from differences in the inventories and not from differences in the models, which supports indications in the recent literature that fossil fuel related emissions might be overestimated in EDGAR. We note that measurements at Cabauw reflect only one limited region of the European domain, and given the many degrees of freedom (transport, source signatures used in the models, emission inventories), one single dataset is not sufficient to make a final decision on the quality of the emission dataset. High frequency analysis of $\delta^{13}C$- and δD at several locations would allow better constraints on isotope source signatures and emissions in atmospheric models. Our proof-of-concept study presented here using continuous high-resolution techniques shows that this will be feasible in the future.

Acknowledgements

712 This project was funded by the European Community's Seventh Framework
713 Program (FP7/2007-2013) within the InGOS project under grant agreement No.
714 284274. Additional funding from the Swiss National Science Foundation (SNSF)
715 within grant No. 200021_134611 and TNA grants within INGOS is gratefully
716 acknowledged. The campaign at the Cabauw tall tower was made possible with
717 strong support from Marcel Brinkenberg (KNMI), Michel Bolder and Henk
718 Snellen (IMAU). We also thank Marco Weber (Empa) for assistance during
719 transport and setup of the TREX-QCLAS system at the CESAR site.

720 **Author contributions**

721 S.E. and C.vdV. carried out the isotope measurements at the Cabauw tower.
722 C.vdV., T.R. and W.A.B. developed the IRMS system. S.E., B.T., L.E. and J.M.
723 developed the TREX-QCLAS system. C.vdV., S.E., J.M., T.R., B.T., M.E.P., G.Z., D.L.,
724 E.G.N., and J.M.N. contributed to the Cabauw measurement campaign. G.M., S.H.
725 and D.B. performed the modeling with TM5 and FLEXPART-COSMO. S.E., T.R.,
726 J.M., B.T., E.H., D.B., G.M., S.H., C.vdV., M.E.P. and H.F. performed and contributed
727 to the data evaluation. S.E. produced the figures for the manuscript. T.R., S.E. and
728 J.M. wrote the manuscript with input from C.vdV., G.M., S.H., E.H., D.B., H.F. and
729 L.E. T.R., L.E. and J.M. designed the study as part of the INGOS project.

730 **Table 1** European CH_4 emissions and isotope source signatures ($\delta^{13}C$, δD) for the
731 different source categories used in TM5.

Process	Yearly emissions (Europe, Tg CH_4/yr)	source signature $\delta^{13}C$/‰
Natural emissions	**22.1**	**-59.2**
Natural wetlands (1)		
Peatland	9.3	-68
Wet mineral soils	4.6	-65
Inundated wetlands	1.3	-60
Geological emissions (2)	6.5	-42
Termites (3)	0.4	-63
Anthropogenic emissions	**45.3**	**-52.4**
Biomass burning (4)	0,3	-23.6
Agriculture (5)		
Domestic ruminants	11	-64
Manure	3	-54
Rice paddies	0.17	-65
Energy sector (5)		
Coal mining	3.4	-47
Oil production	3	-42
Gas production and distribution	12	-42
Oil combustion	0.41	-32
Residential sector (5)	1.6	-32
Waste treatment (5)		
Landfills	9	-54
Waste waters	3	-50
Total	**67.4**	**-54.6**

732 (1) Spahni et al. (2011); (2) Etiope et al. (2008); (3) Sanderson et al. (1996); (4)
733 GFED3/4 (http://www.globalfiredata.org/); (5) EDGAR4.2FT (EDGAR, 2010).
734

735 **Table 2** SNAP (Standardized Nomenclature for Air Pollutants) source categories
736 and corresponding $\delta^{13}C$ and δD source signatures from the TNO-MACC_2
737 inventory as used in FLEXPART-COSMO.

SNAP Category	Description	$\delta^{13}C$/‰	δD/‰
1	Energy industries, oil or gas production	-42	-175
2	Residential combustion	-32	-175
3+4	Industrial combustion and non-combustion processes	-60	-175
5	Extraction and distribution of fossil fuels including distribution of natural gas	-42	-175
7	Road transport	-20	-175
9	Waste including emissions from landfills	-54	-293
10	Agriculture including emissions from ruminants and manure management	-64	-319
6+8	Other emissions (negligible)	-42	-175

738

739 **Table 3**. Mean value and standard deviation of the histograms of the source
740 isotopic composition shown in Fig. 10.

Model + Inventory	**Method**	**$\delta^{13}C$/‰**	**δD/‰**
Measurement data	MKP	-61.0 ± 2.8	-300 ± 22
TM5 + Edgar	MKP	-53.3 ± 1.1	
FLEXPART-COSMO + Edgar	MKP	-54.5 ± 1.6	-277 ± 10
FLEXPART-COSMO + Edgar	Direct	-53.4 ± 1.7	-269 ± 10
TM5 + TNO-MACC	MKP	-56.7 ± 0.8	
FLEXPART-COSMO + TNO-MACC	MKP	-57.6 ± 1.9	-294 ± 12
FLEXPART-COSMO + TNO-MACC	Direct	-57.2 ± 1.7	-289 ± 11

741

742 **Figures**

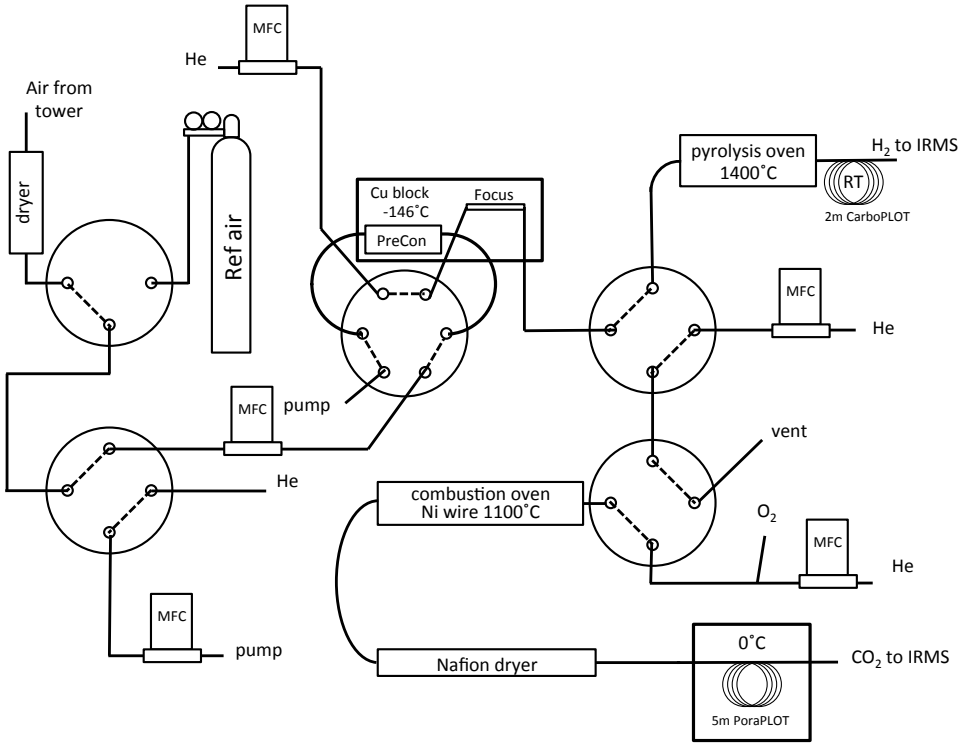

743 Fig. 1: Schematics of the pre-concentration and extraction system developed for
744 the IRMS technique. MFC denotes mass flow controller. The 8-port valve through
745 which the Ref air bottle was connected to the first selection valve is not shown to
746 reduce complexity. For further description see the main text.

747

748

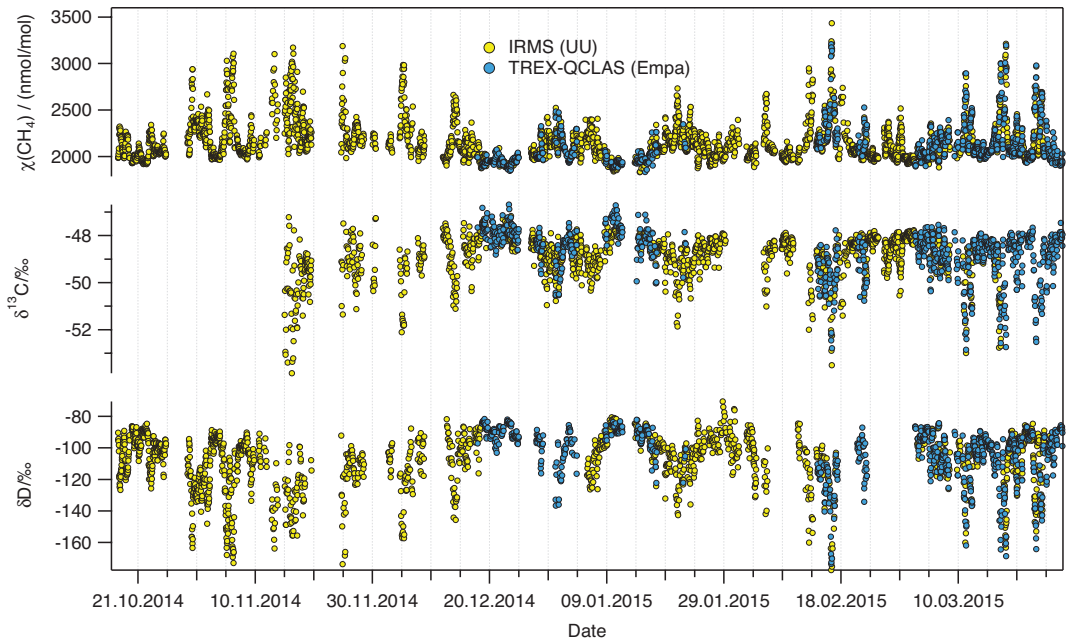

Fig. 2.: CH_4 mole fraction, $\chi(CH_4)$, and isotopic composition ($\delta^{13}C$, δD) measured at the Cabauw tall tower from 17 October 2014 until 29 March 2015. Real-time measurements by IRMS (Utrecht University) are indicated in yellow, TREX-QCLAS (Empa) data in blue.

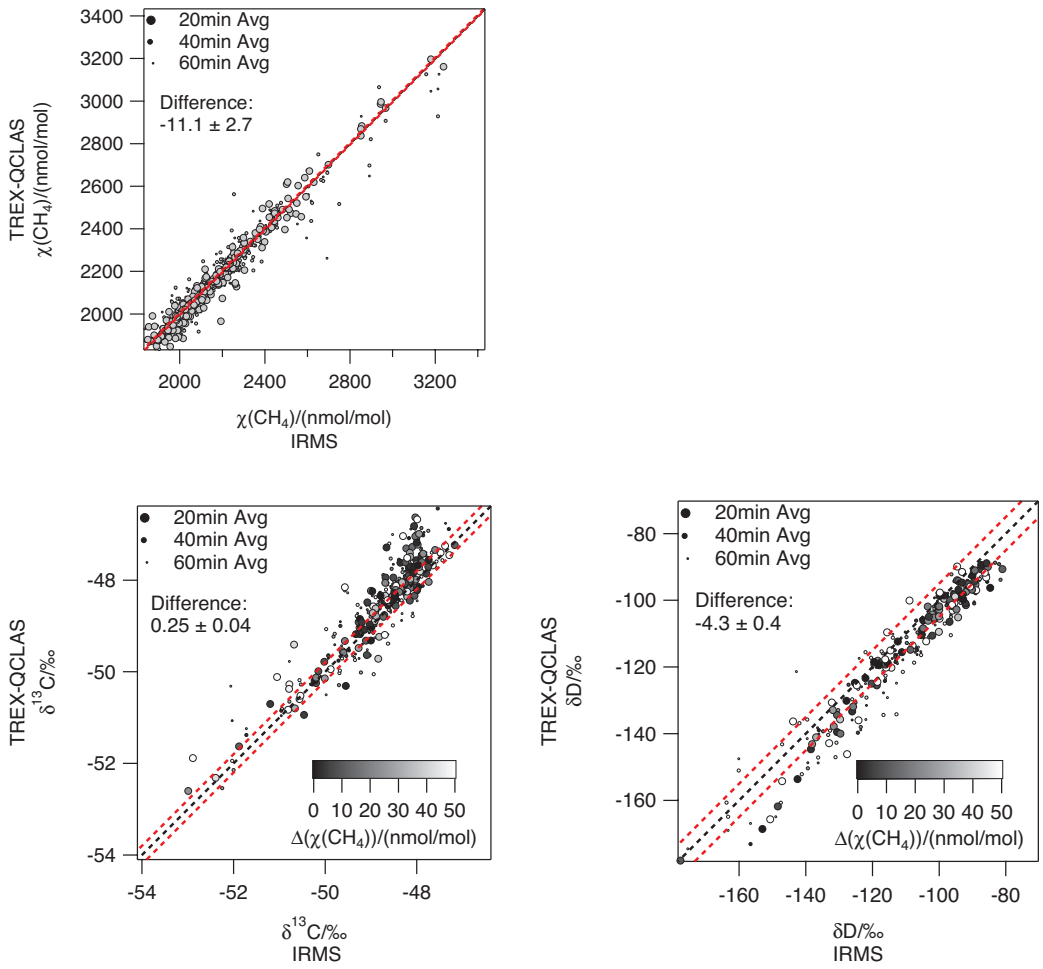

Fig. 2: Correlation diagrams for CH_4 mole fraction, $\delta^{13}C$ and δD analyzed with IRMS (Utrecht University) and TREX-QCLAS (Empa). The dashed black lines are 1:1 lines, dashed red lines mark the extended WMO compatibility goals of ± 5 nmol/mol, ± 0.2 ‰ and ± 5 ‰ for CH_4 mole fraction, $\delta^{13}C$ and δD, respectively. The temporal difference between IRMS and TREX-QCLAS sampling is indicated by the point size (large: 20 min, medium: 40 min, small: 60 min). For $\delta^{13}C$ and δD, the differences in the CH_4 mole fraction of the measurements are represented by the shading (black: identical mole fractions, white: 50 nmol/mol difference).

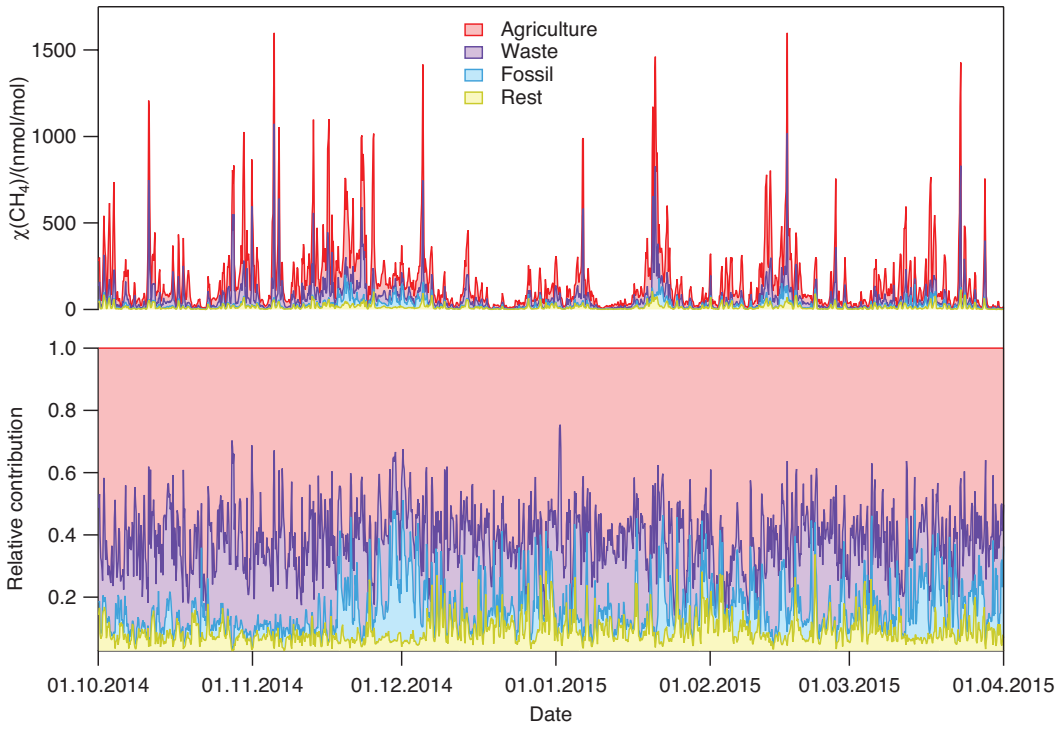

Fig. 3: Absolute (top) and relative (bottom) contributions of methane emissions that are picked up along the 4-day FLEXPART-COSMO trajectories during the campaign. The results shown are from the FLEXPART-COSMO simulations with the TNO-MACC inventory. They indicate major contributions of the following source categories: “agriculture” (mainly ruminants), “waste” (mainly landfills) and “fossil” (fugitive losses from coal, oil and natural gas production and from gas transportation and distribution) to the increase in CH_4 mole fractions at Cabauw. The category “rest” primarily represents residential CH_4 emissions.

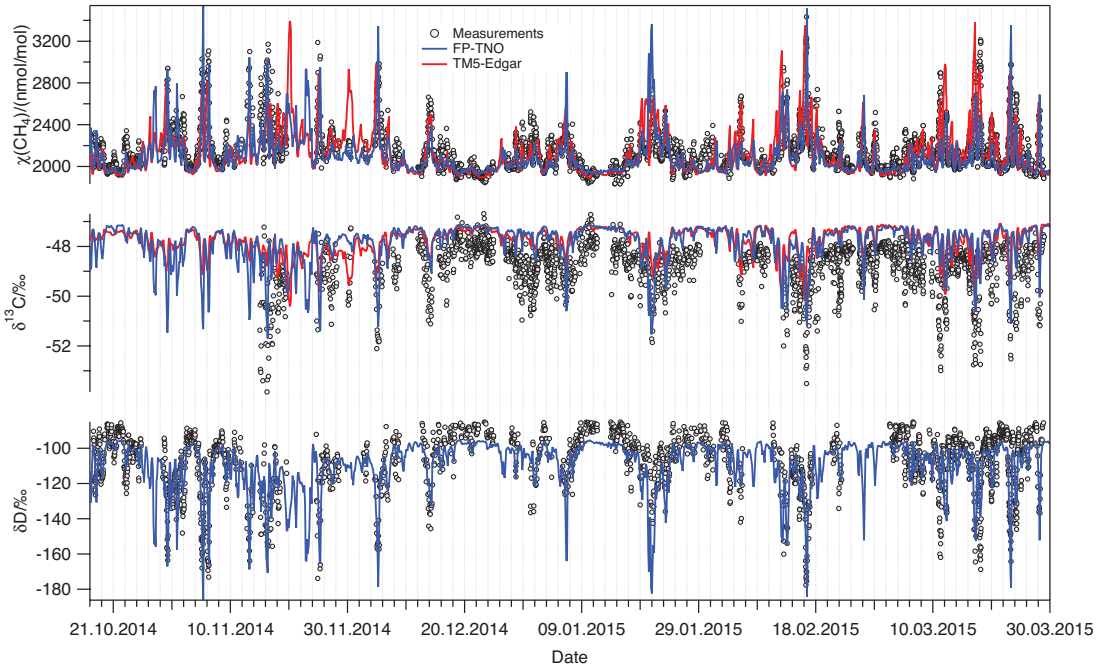

780

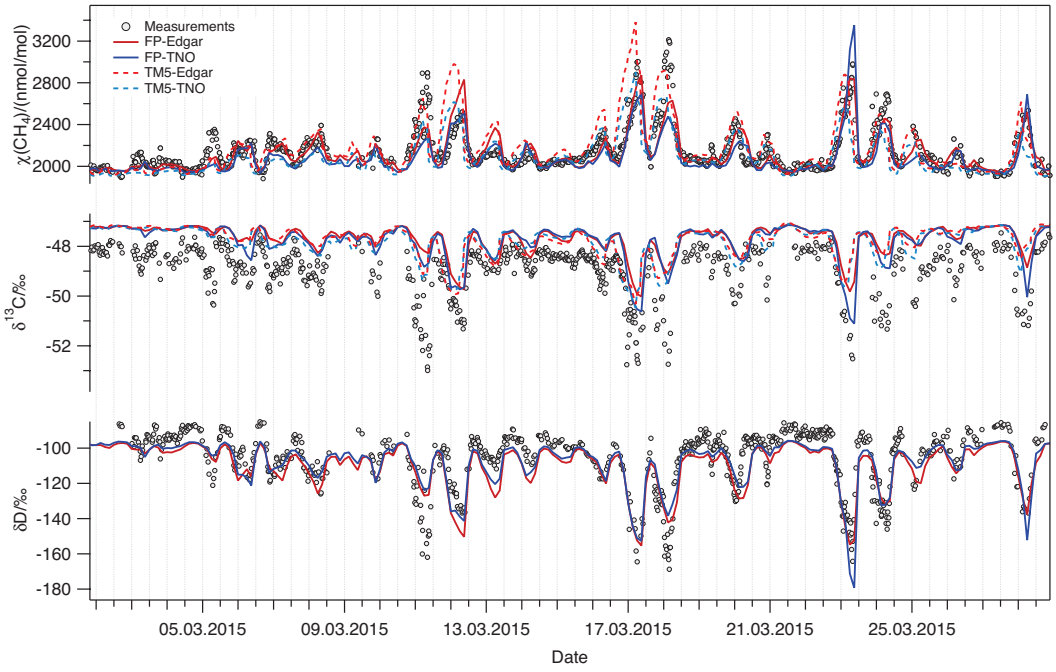

781

782 Fig. 4: Comparison of the modeled and measured time series of CH_4 mole fraction
783 and isotopic composition ($\delta^{13}C$- and δD). Measurements are shown as circles and
784 model results as lines. Top graph: two selected model configurations for the
785 entire campaign: FLEXPART-COSMO using the TNO-MACC inventory (blue) and
786 TM5 using the Edgar/Why-Me inventory (red). Bottom graph: Time series for
787 March 2015 with all four model – inventory combinations. For δD, only the
788 synthetic FLEXPART-COSMO results are available for comparison since TM5
789 does not simulate δD.

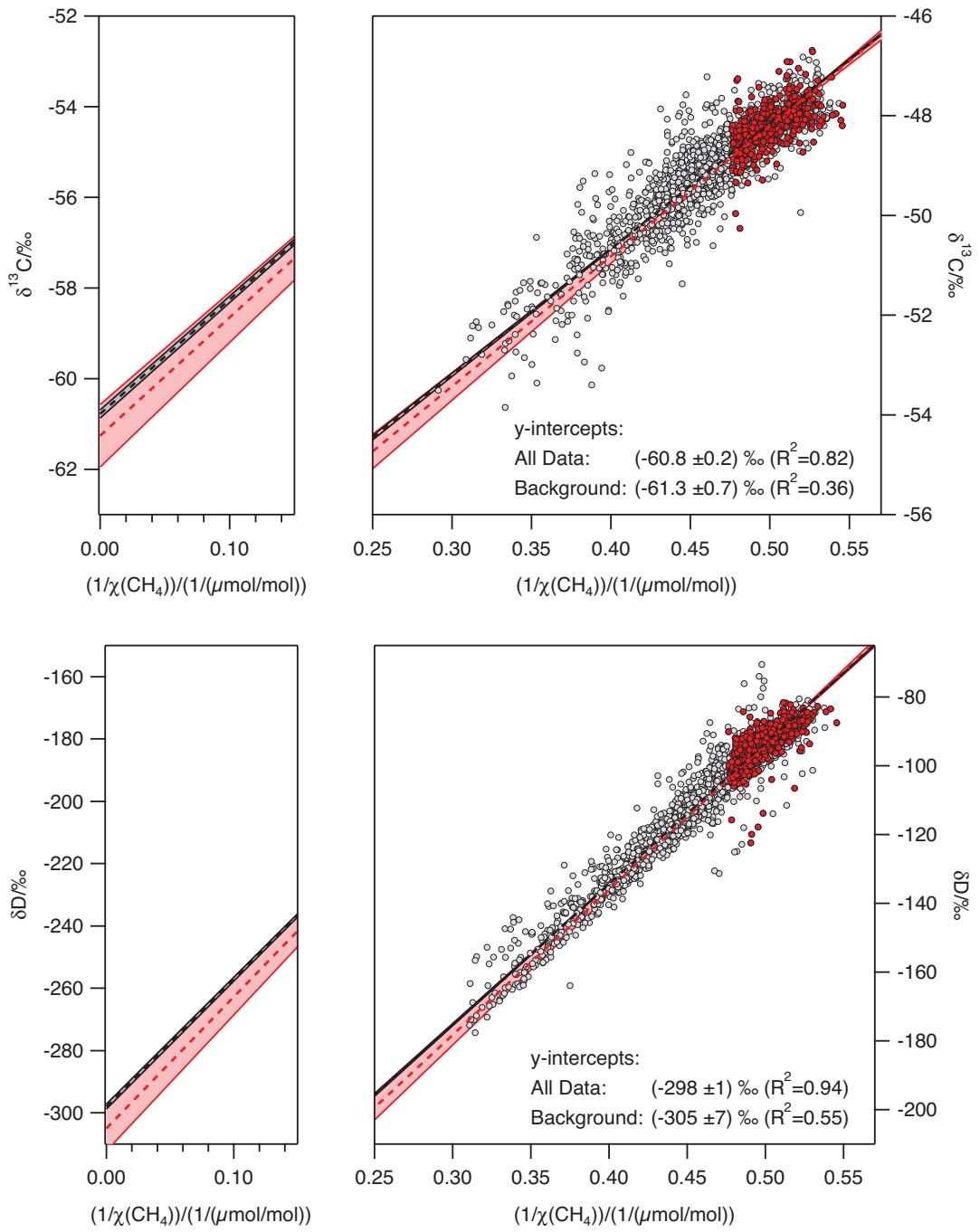

Fig. 5: Keeling plot of all data using an orthogonal regression method. The dashed line indicates the regression line and the shaded area the confidence interval taking into account the measurement uncertainties. The color code indicates all measured data (grey points) and daily background values (red points). Left panels show the region near the y-axis intercept.

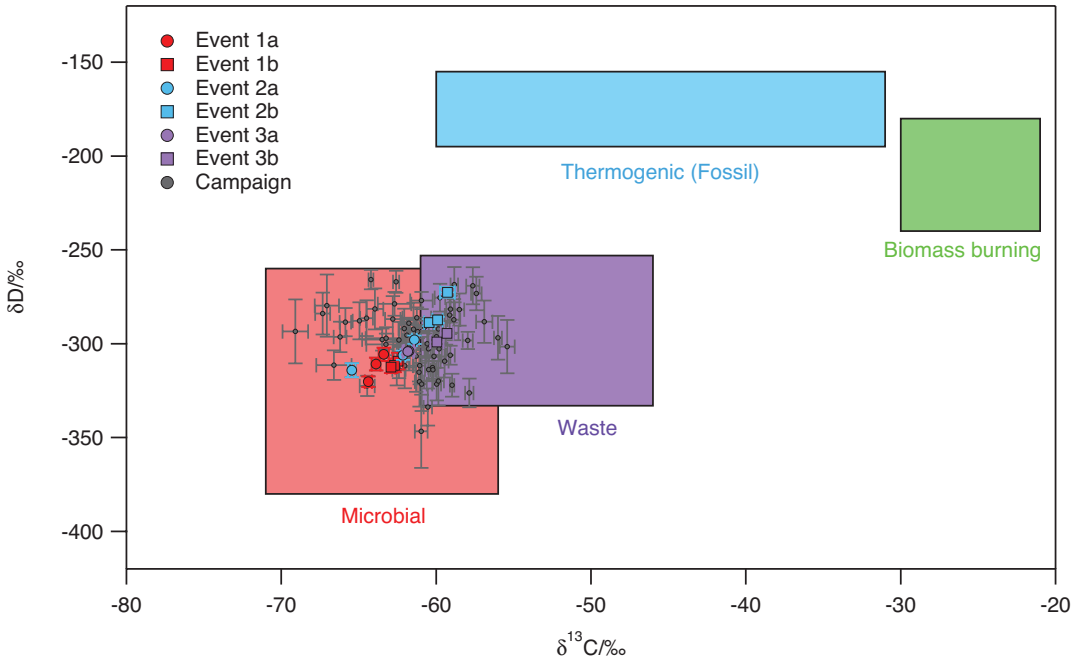

Fig. 6: MKP intercepts of δD vs. $\delta^{13}C$. The colored areas indicate typical isotope signatures for different source categories. Circles show the 6h-averaged source signatures. Large colored symbols indicate data from the three events (event 1: 10th – 12th March, event 2: 16th – 18th March, event 3: 22nd to 24th March) that are highlighted in Fig. 9. The labels a and b refer to day 1 and day 2 of the two-day events, respectively. For the source signatures, the $\delta^{13}C$ values are taken from Table 1 and the δD values from recent literature (Snover et al., 2000; Rigby et al., 2012).

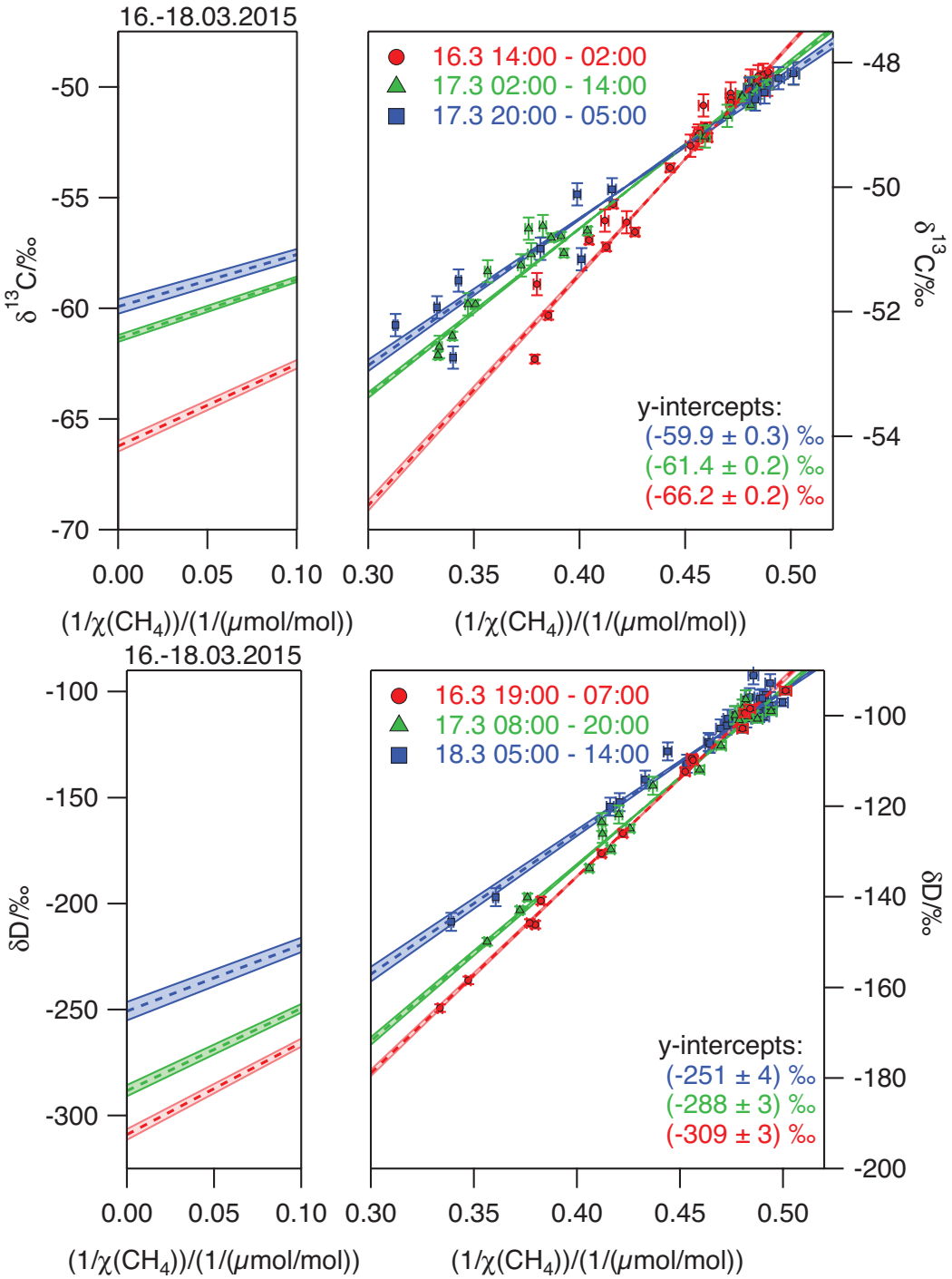

Fig. 7: Keeling plots for the period between 16 and 18 March, illustrating a rapid change in δ values over the course of hours, which is most probably related to a change from mainly ruminant derived CH_4 to a significant contribution of fossil and/or waste CH_4. The dashed lines indicate the regression line, the shaded areas show the uncertainty (one standard deviation) of the regression line. Left panels show the region near the y-axis intercept. Times indicated are Central European Time (CET).

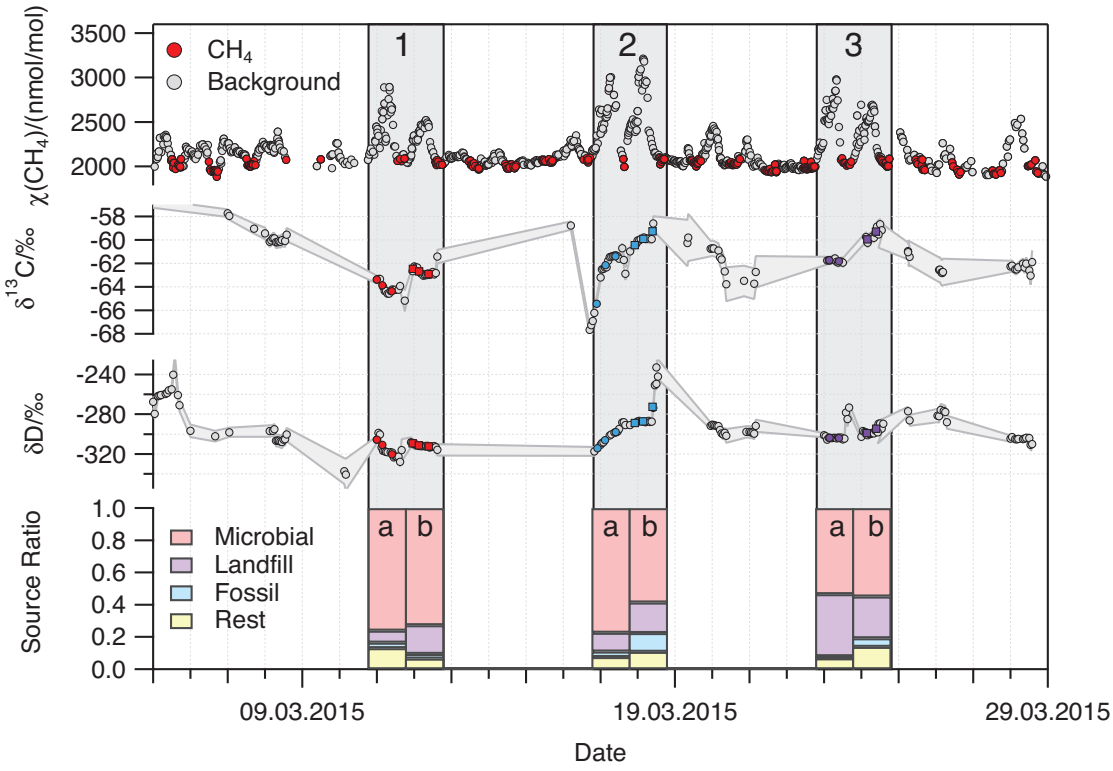

Fig. 8: Detailed analysis of three 2-day periods with large CH_4 elevations in March 2015. The top panel exhibits CH_4 mole fraction (grey) with background values in red (10:00-18:00, >2100 nmol/mol). The middle panels show the mean isotopic signatures ($\delta^{13}C$, δD) derived with the 12-h MKP method. The color-coding in the middle panels (red, light blue, purple) indicates characteristic contributions from different sources; red-microbial, light blue-fossil, purple-waste. For consistency, the same color-coding was chosen in Fig. 7. The bottom graph presents CH_4 source contributions as computed with the FLEXPART-COSMO model using the TNO-MACC inventory, averaged over 24 hours.

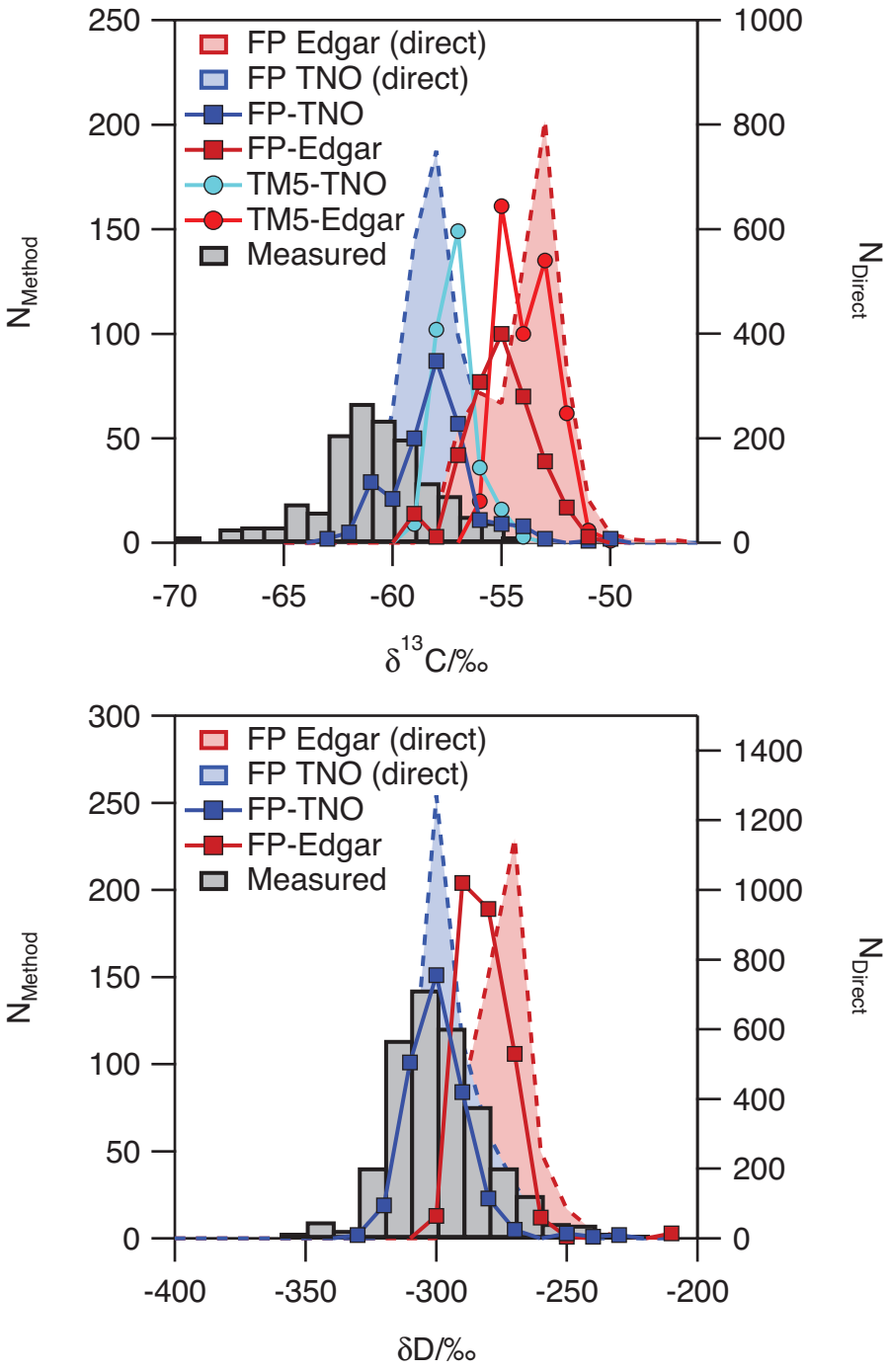

Fig. 10: Histograms of CH_4 isotope source signatures at the CESAR site between October 2014 and March 2015. Bin widths are 1 ‰ for $\delta^{13}C$ and 10 ‰ for δD. Mean isotopic signatures are derived from measured data (grey bins), FLEXPART-COSMO modeling (squares) as well as TM5 modeling (circles) using the 12 h MKP method. Two different inventories, TNO-MACC (blue) and

Edgar/LPJ-Why-Me (red), were used. The shaded areas show histograms for the "direct" source signatures that were picked up along the FLEXPART-COSMO trajectory (right axis).

References

Baertschi, P.: Absolute 18O content of Standard Mean Ocean Water, Earth Planet. Sci. Lett., 31, 341-344, 1976.

Baldauf, M., Seifert, A., Förstner, J., Majewski, D., Raschendorfer, M., and Reinhardt, T.: Operational Convective-Scale Numerical Weather Prediction with the COSMO Model: Description and Sensitivities, Monthly Weather Review, 139, 3887–3905, doi:3810.1175/MWR-D-3810-05013.05011, 2011.

Beck, V., Chen, H. L., Gerbig, C., Bergamaschi, P., Bruhwiler, L., Houweling, S., Röckmann, T., Kolle, O., Steinbach, J., Koch, T., Sapart, C. J., van der Veen, C., Frankenberg, C., Andreae, M. O., Artaxo, P., Longo, K. M., and Wofsy, S. C.: Methane airborne measurements and comparison to global models during BARCA, J. Geophys. Res., 117, D15310, doi:15310.11029/12011JD017345, 2012.

Bergamaschi, P., Brenninkmeijer, C. A. M., Hahn, M., Röckmann, T., Scharffe, D. H., Crutzen, P. J., Elansky, N. F., Belikov, I. B., Trivett, N. B. A., and Worthy, D. E. J.: Isotope analysis based source identification for atmospheric CH_4 and CO across Russia using the Trans-Siberian railroad, J. Geophys. Res., 103, D7, 8227-8235, DOI: 8210.1029/8297JD03738, 1998a.

Bergamaschi, P., Houweling, S., Segers, A., Krol, M., Frankenberg, C., Scheepmaker, R. A., Dlugokencky, E., Wofsy, S. C., Kort, E. A., Sweeney, C., Schuck, T., Brenninkmeijer, C., Chen, H., Beck, V., and Gerbig, C.: Atmospheric CH_4 in the first decade of the 21st century: Inverse modeling analysis using SCIAMACHY satellite retrievals and NOAA surface measurements, J Geophys Res-Atmos, 118, 7350–7369, doi:7310.1002/jgrd.50480, 2013.

Bergamaschi, P., Lubina, C., Konigstedt, R., Fischer, H., Veltkamp, A. C., and Zwaagstra, O.: Stable isotopic signatures ($\delta^{13}C$, δD) of methane from European landfill sites, J. Geophys. Res., 103, 8251-8265, doi 8210.1029/8298jd00105, 1998b.

Bergamaschi, P., Schupp, M., and Harris, G. W.: High-precision direct measurements of $^{13}CH_4/^{12}CH_4$ and $CH_3D/^{12}CH_4$ ratios in atmospheric methane sources by means of a long-path tunable diode laser absorbtion spectrometer, Appl. Opt., 33, No.33, 7704-7716, 1994.

Bock, M., Schmitt, J., Behrens, M., Moller, L., Schneider, R., Sapart, C., and Fischer, H.: A gas chromatography/pyrolysis/isotope ratio mass spectrometry system for high-precision δD measurements of atmospheric methane extracted from ice cores, Rap. Commun. Mass Spectrom., 24, 621-633, 2010.

Brass, M. and Röckmann, T.: Continuous-flow isotope ratio mass spectrometry method for carbon and hydrogen isotope measurements on atmospheric methane, Atmos. Meas. Tech., 3, 1707-1721, 2010.

Brenninkmeijer, C. A. M., Lowe, D. C., Manning, M. R., Sparks, R. J., and Velthoven, P. F. J. v.: The ^{13}C, ^{14}C, and ^{18}O isotopic composition of CO, CH_4 and CO_2 in the higher southern latitudes lower stratosphere, J. Geophys. Res., 100, 26,163-126,172, 1995.

Bruhwiler, L., Dlugokencky, E., Masarie, K., Ishizawa, M., Andrews, A., Miller, J., Sweeney, C., Tans, P., and Worthy, D.: CarbonTracker-CH_4: an assimilation system for estimating emissions of atmospheric methane, Atmos. Chem. Phys., 14, 8269-8293, 2014.

Craig, H.: Isotopic standards for carbon and oxygen and correction factors for mass-spectrometric analysis of carbon dioxide, Geochim. Cosmochim. Acta, 12, 133-149, 1957.

Dee, D. P., Uppala, S. M., Simmons, A. J., Berrisford, P., Poli, P., and al., e.: The ERA-Interim reanalysis: configuration and performance of the data assimilation system, Quart. J. Roy. Meteor. Soc., 553-579, 2011.

Dlugokencky, E. J., Bruhwiler, L., White, J. W. C., Emmons, L. K., Novelli, P. C., Montzka, S. A., Masarie, K. A., Lang, P. M., Crotwell, A. M., Miller, J. B., and Gatti, L. V.: Observational constraints on recent increases in the atmospheric CH_4 burden, Geophys. Res. Lett., 36, L18803, doi 18810.11029/12009gl039780, 2009.

Dlugokencky, E. J., Dutton, E. G., Novelli, P. C., Tans, P. P., Masarie, K. A., Lantz, K. O., and Madronich, S.: Changes in CH_4 and CO growth rates after the eruption of Mt. Pinatubo and their link with changes in tropical tropospheric UV flux, Geophys. Res. Lett., 23, 2761-2764, 1996.

Dlugokencky, E. J., Masarie, K. A., Lang, P. M., and Tans, P. P.: Continuing decline in the growth rate of the atmospheric methane burden, Nature, 393, 447-450, 1998.

Dlugokencky, E. J., Myers, R. C., Lang, P. M., Masarie, K. A., Crotwell, A. M., Thoning, K. W., Hall, B. D., Elkins, J. W., and Steele, L. P.: Conversion of NOAA atmospheric dry air CH_4 mole fractions to a gravimetrically prepared standard scale, J. Geophys. Res., 110, D18306, Doi 18310.11029/12005jd006035, 2005.

EDGAR: European Commission, Joint Research Centre (JRC)/Netherlands Environmental Assessment Agency (PBL). , Emission Database for Global Atmospheric Research (EDGAR), Version 4.2. , 2010. Available at http://edgar.jrc.ec.europa.eu., 2010.

EDGAR: European Commission, Joint Research Centre (JRC)/Netherlands Environmental Assessment Agency (PBL). Emission Database for Global Atmospheric Research (EDGAR), release version 4.2. http://edgar.jrc.ec.europe.eu., 2009.

Etheridge, D. M., Steele, L. P., Francey, R. J., and Langenfelds, R. L.: Atmospheric methane between 1000 AD and present: Evidence of antropogenic emissions and climatic variability, J. Geophys. Res., 103, 15979-15993, 1998.

Etiope, G., Lassey, K. R., Klusman, R. W., and Boschi, E.: Reappraisal of the fossil methane budget and related emission from geologic sources, Geophys. Res. Lett., 35, 2008.

Eyer, S. and al, e.: Real-time analysis of $\delta^{13}C$- and δD-CH_4 in ambient air with laser spectroscopy: Method development and first intercomparison results., Atmos. Meas. Tech. Discuss., 8, 8925-8970, 2015.

Eyer, S., Stadie, N. P., Borgschulte, A., Emmenegger, L., and Mohn, J.: Methane preconcentration by adsorption: a methodology for materials and conditions selection, Adsorption-Journal of the International Adsorption Society, 20, 657-666, 2014.

Ferretti, D., Miller, J., White, J., Etheridge, D., Lassey, K., Lowe, D., Allan, B., MacFarling, C., Dreier, M., Trudinger, C., and Ommen, T. v.: Unexpected changes to the global methane budget over the past 2000 years, Science, 309, 1714-1717, 2005.

Fischer, H., Behrens, M., Bock, M., Richter, U., Schmitt, J., Loulergue, L., Chappellaz, J., Spahni, R., Blunier, T., Leuenberger, M., and Stocker, T. F.: Changing boreal methane sources and constant biomass burning during the last termination, Nature, 452, 864-867, 2008.

Gros, V., Brenninkmeijer, C. A. M., Jöckel, P., Kaiser, J., Lowry, D., Nisbet, E. G., O'Brian, P., Röckmann, T., and Warwick, N.: Isotope signatures of trace gas sources. In: Emissions Of Atmospheric Trace Compounds, Granier, C., Artaxo, P., and Reeves, C. E. (Eds.), Advances in Global Change Research, Kluwer Academic Pub., Paris, 2004.

Henne, S., Brunner, D., Oney, B., Leuenberger, M., Eugster, W., Bamberger, I., Meinhardt, F., Steinbacher, M., and Emmenegger, L.: Validation of the Swiss methane emission inventory by atmospheric observations and inverse modelling, Atmos. Chem. Phys. Discuss., 2015. 35417-35484, doi:35410.35194/acpd-35415-35417-32015, 2015.

Hiller, R. V., Bretscher, D., DelSontro, T., Diem, T., Eugster, W., Henneberger, R., Hobi, S., Hodson, E., Imer, D., Kreuzer, M., Künzle, T., Merbold, L., Niklaus, P. A., Rihm, B., Schellenberger, A., Schroth, M. H., Schubert, C. J., Siegrist, H., Stieger, J., Buchmann, N., and Brunner, D.: Anthropogenic and natural methane fluxes in Switzerland synthesized within a spatially explicit inventory, Biogeosciences, 11, 1941-1959, doi:1910.5194/bg-1911-1941-2014, 2014.

Houweling, S., Krol, M., Bergamaschi, P., Frankenberg, C., Dlugokencky, E. J., Morino, I., Notholt, J., Sherlock, V., Wunch, D., Beck, V., Gerbig, C., Chen, H., Kort, E. A., Röckmann, T., and Aben, I.: A multi-year methane inversion using SCIAMACHY, accounting for systematic errors using TCCON measurements, Atmos. Chem. Phys., 14, 3991-4012, 2014.

Houweling, S., van der Werf, G. R., Goldewijk, K. K., Röckmann, T., and Aben, I.: Early anthropogenic CH_4 emissions and the variation of CH_4 and $^{13}CH_4$ over the last millennium, Global Biogeochem Cy, 22, 2008.

Kawagucci, S., Kobayashi, M., Hattori, S., Yamada, K., Ueno, Y., Takai, K., and Yoshida, N.: Hydrogen isotope systematics among H_2-H_2O-CH_4 during the growth of the hydrogenotrophic methanogen Methanothermobacter thermautotrophicus strain Delta H, Geochim Cosmochim Ac, 142, 601-614, 2014.

Keeling, C. D.: The Concentration and Isotopic Abundances of Carbon Dioxide in Rural and Marine Air, Geochim. Cosmochim. Acta, 24, 277-298, 1961.

Khalil, M. A. K., Butenhoff, C. L., and Rasmussen, R. A.: Atmospheric methane: Trends and cycles of sources and sinks, Environmental Science & Technology, 41, 2131-2137, 2007.

Kirschke, S., Bousquet, P., Ciais, P., Saunois, M., Canadell, J. G., Dlugokencky, E. J., Bergamaschi, P., Bergmann, D., Blake, D. R., Bruhwiler, L., Cameron-Smith, P., Castaldi, S., Chevallier, F., Feng, L., Fraser, A., Heimann, M., Hodson, E. L., Houweling, S., Josse, B., Fraser, P. J., Krummel, P. B., Lamarque, J. F., Langenfelds, R. L., Le Quere, C., Naik, V., O'Doherty, S., Palmer, P. I., Pison, I., Plummer, D., Poulter, B., Prinn, R. G., Rigby, M., Ringeval, B., Santini, M., Schmidt, M., Shindell, D. T., Simpson, I. J., Spahni, R., Steele, L. P., Strode, S. A., Sudo, K., Szopa, S., van der Werf, G. R., Voulgarakis, A., van Weele, M., Weiss, R. F., Williams, J. E., and

Zeng, G.: Three decades of global methane sources and sinks, Nat Geosci, 6, 813-823, 2013.

Klevenhusen, F., Bernasconi, S. M., Kreuzer, M., and Soliva, C. R.: Experimental validation of the Intergovernmental Panel on Climate Change default values for ruminant-derived methane and its carbon-isotope signature, Anim Prod Sci, 50, 159-167, 2010.

Krol, M., Houweling, S., Bregman, B., van den Broek, M., Segers, A., van Velthoven, P., Peters, W., Dentener, F., and Bergamaschi, P.: The two-way nested global chemistry-transport zoom model TM5: algorithm and applications, Atmos. Chem. Phys., 5, 417-432, 2005.

Kuenen, J. J. P., Visschedijk, A. J. H., Jozwicka, M., and van der Gon, H. A. C. D.: TNO-MACC_II emission inventory; a multi-year (2003-2009) consistent high-resolution European emission inventory for air quality modelling, Atmos. Chem. Phys., 14, 10963-10976, 2014.

Lassey, K. R., Lowe, D. C., Brenninkmeijer, C. A. M., and Gomez, A. J.: Atmospheric Methane and its Carbon Isotopes in the Southern Hemnisphere: their Time Series and an Instructive Model, Chemosphere, 26, 95-109, 1993.

Lassey, K. R., Lowe, D. C., and Manning, M. R.: The trend in atmospheric methane $\delta^{13}C$ implications for isotopic constraints on the global methane budget, Global Biogeochem Cy, 14, 41-49, 2000.

Loulergue, L., Schilt, A., Spahni, R., Masson-Delmotte, V., Blunier, T., Lemieux, B., Barnola, J. M., Raynaud, D., Stocker, T. F., and Chappellaz, J.: Orbital and millennial-scale features of atmospheric CH_4 over the past 800,000 years, Nature, 453, 383-386, 2008.

Lowe, D. C., Brenninkmeijer, C. A. M., Brailsford, G. W., Lassey, K. R., Gomez, A. J., and Nisbet, E. G.: Concentration and ^{13}C Records of Atmospheric Methane in New-Zealand and Antarctica - Evidence for Changes in Methane Sources, J. Geophys. Res., 99, 16913-16925, 1994.

MacFarling Meure, C., Etheridge, D., Trudinger, C., Steele, P., Langenfelds, R., Ommen, T. v., Smith, A., and Elkins, J.: Law Dome CO_2, CH_4 and N_2O ice core records extended to 2000 years BP Geophys. Res. Lett., 33, L14810, doi:14810.11029/12006GL026152 2006.

Merritt, D. A., Brand, W. A., and Hayes, J. M.: Isotope-ratio-monitoring gas chromatography-mass spectrometry: methods for isotopic calibration, Org. Geochem., 21 No. 6/7, 573-583, 1994.

Merritt, D. A., Hayes, J. M., and Des Marais, D. J.: Carbon isotopic analysis of atmospheric methane by isotope-ratio-monitoring gas chromatography-mass spectrometry, J. Geophys. Res., 100 D, 1317-1326, 1995.

Mohn, J., Guggenheim, C., Tuzson, B., Vollmer, M. K., Toyoda, S., Yoshida, N., and Emmenegger, L.: A liquid nitrogen-free preconcentration unit for measurements of ambient N2O isotopomers by QCLAS, Atmos Meas Tech, 3, 609-618, 2010.

Mohn, J., Tuzson, B., Manninen, A., Yoshida, N., Toyoda, S., Brand, W. A., and Emmenegger, L.: Site selective real-time measurements of atmospheric N_2O isotopomers by laser spectroscopy, Atmos Meas Tech, 5, 1601-1609, 2012.

Monteil, G., Houweling, S., Dlugockenky, E. J., Maenhout, G., Vaughn, B. H., White, J. W. C., and Röckmann, T.: Interpreting methane variations in the past two

decades using measurements of CH_4 mixing ratio and isotopic composition, Atmos. Chem. Phys., 11, 9141-9153, 2011.

Monteil, G., Houweling, S., Guerlet, S., Schepers, D., Frankenberg, C., Scheepmaker, R., Aben, I., Butz, A., Hasekamp, O., Landgraf, J., Wofsy, S. C., and Röckmann, T.: Intercomparison of 15 months inversions of GOSAT and SCIAMACHY CH4 retrievals, J. Geophys. Res., 118, 11807-11823, doi:11810.11002/12013JD019760, 2013.

Nisbet, E. G., Dlugokencky, E. J., and Bousquet, P.: Methane on the rise—again, Science, 343, 493-495, 2014.

Pataki, D. E., Ehleringer, J. R., Flanagan, L. B., Yakir, D., Bowling, D. R., Still, C. J., Buchmann, N., Kaplan, J. O., and Berry, J. A.: The application and interpretation of Keeling plots in terrestrial carbon cycle research, Global Biogeochem Cy, 17, 1022, doi:1010.1029/2001GB001850, 2003.

Peltola, O., Hensen, A., Helfter, C., Marchesini, L. B., Bosveld, F. C., van den Bulk, W. C. M., Elbers, J. A., Haapanala, S., Holst, J., Laurila, T., Lindroth, A., Nemitz, E., Röckmann, T., Vermeulen, A. T., and Mammarella, I.: Evaluating the performance of commonly used gas analysers for methane eddy covariance flux measurements: the InGOS inter-comparison field experiment, Biogeosciences, 11, 3163-3186, 2014.

Peltola, O., Hensen, A., Marchesini, L. B., Helfter, C., Bosveld, F. C., van den Bulk, W. C. M., Haapanala, S., van Huissteden, J., Laurila, T., Lindroth, A., Nemitz, E., Röckmann, T., Vermeulen, A. T., and Mammarella, I.: Studying the spatial variability of methane flux with five eddy covariance towers of varying height, Agricultural and Forest Meteorology, 214, 456-472, 2015.

Quay, P., Stutsman, J., Wilbur, D., Snover, A., Dlugokencky, E., and Brown, T.: The isotopic composition of atmospheric methane, Global Biogeochem Cy, 13, 445-461, 1999.

Rasmussen, R. A. and Khalil, M. A. K.: Atmospheric Methane (CH_4) - Trends and Seasonal Cycles, J. Geophys. Res., 86, 9826-9832, 1981.

Rigby, M., Manning, A. J., and Prinn, R. G.: The value of high-frequency, high-precision methane isotopologue measurements for source and sink estimation, J. Geophys. Res., 117, 2012.

Röckmann, T., Brass, M., Borchers, R., and Engel, A.: The isotopic composition of methane in the stratosphere: High-altitude balloon sample measurements, Atm. Chem. Phys., 11, 13287-13304, 2011.

Sanderson, M. G.: Biomass of termites and their emissions of methane and carbon dioxide: A global database, Global Biogeochem. Cycles, 10, 543–557, 1996.

Sapart, C. J., Monteil, G., Prokopiou, M., van de Wal, R. S. W., Kaplan, J. O., Sperlich, P., Krumhardt, K. M., van der Veen, C., Houweling, S., Krol, M. C., Blunier, T., Sowers, T., Martinerie, P., Witrant, E., Dahl-Jensen, D., and Röckmann, T.: Natural and anthropogenic variations in methane sources during the past two millennia, Nature, 490, 85-88, 2012.

Sapart, C. J., Veen, C. v. d., Vigano, I., Brass, M., Wal, R. S. W. v. d., Bock, M., Fischer, H., Sowers, T., Buizert, C., Sperlich, P., Blunier, T., Behrens, M., Schmitt, J., Seth, B., and Röckmann, T.: Simultaneous stable isotope analysis of methane and nitrous oxide on ice core samples, Atmos. Meas. Tech., 4, 2607-2618, 2011.

1076 Saueressig, G., Bergamaschi, P., Crowley, J. N., Fischer, H., and Harris, G. W.:
1077 D/H kinetic isotope effect in the reaction CH_4 + Cl, Geophys. Res. Lett., 23, 3619-
1078 3622, 1996.
1079 Saueressig, G., Crowley, J. N., Bergamaschi, P., Brühl, C., Brenninkmeijer, C. A.
1080 M., and Fischer, H.: Carbon 13 and D kinetic isotope effects in the reactions of CH_4
1081 with $O(^1D)$ and OH: New laboratory measurements and their implications for the
1082 isotopic composition of stratospheric methane, J. Geophys. Res., 106, 23127-23138,
1083 2001.
1084 Schmitt, J., Seth, B., Bock, M., van der Veen, C., Möller, L., Sapart, C. J.,
1085 Prokopiou, M., Sowers, T., Röckmann, T., and Fischer, H.: On the interference of Kr
1086 during carbon isotope analysis of methane using continuous-flow combustion-isotope
1087 ratio mass spectrometry, Atmos. Meas. Tech., 6, 1425-1445, 2013.
1088 Seibert, P. and Frank, A.: Source-receptor matrix calculation with a Lagrangian
1089 particle dispersion model in backward mode, Atmos. Chem. Phys., 4, 51-63, 2004.
1090 Snover, A. K. and Quay, P. D.: Hydrogen and carbon kinetic isotope effects
1091 during soil uptake of atmospheric methane, Global Biogeochem. Cycles, 14, 25-39,
1092 2000.
1093 Spahni, R., Chappellaz, J., Stocker, T. F., Loulergue, L., Hausammann, G.,
1094 Kawamura, K., Flückiger, J., Schwander, J., Raynaud, D., Masson-Delmotte, V., and
1095 Jouzel, J.: Atmospheric Methane and Nitrous Oxide of the Late Pleistocene from
1096 Antarctic Ice Cores, Science, 310, 1317-1321, DOI: 1310.1126/science.1120132,
1097 2005.
1098 Spahni, R., Wania, R., Neef, L., Weele, M. v., Pison, I., Bousquet, P.,
1099 Frankenberg, C., Foster, P. N., Joos, F., Prentice, I. C., and Velthoven, P. v.:
1100 Constraining global methane emissions and uptake by ecosystems, Biogeosciences, 8,
1101 1643–1665, doi:1610.5194/bg-1648-1643-2011., 2011.
1102 Sperlich, P., Buizert, C., Jenk, T. M., Sapart, C. J., Prokopiou, M., Rockmann, T.,
1103 and Blunier, T.: An automated GC-C-GC-IRMS setup to measure palaeoatmospheric
1104 $\delta^{13}C$-CH_4, $\delta^{15}N$-N_2O and $\delta^{18}O$-N_2O in one ice core sample, Atmos Meas Tech, 6,
1105 2027-2041, 2013.
1106 Sperlich, P., Uitslag, N. A. M., Richter, J. M., Rothe, M., Geilmann, H., Veen, C.
1107 v., Röckmann, T., Blunier, T., and Brand, W. A.: Development and evaluation of a
1108 suite of isotope reference gases for methane in air, submitted to Atmos. Meas. Tech.
1109 Disc., 2016. 2016.
1110 Stohl, A., Forster, C., Frank, A., Seibert, P., and Wotawa, G.: Technical note: The
1111 Lagrangian particle dispersion model FLEXPART version 6.2, Atmos. Chem. Phys.,
1112 5, 2461-2474, 2005.
1113 Sturm, P., Tuzson, B., Henne, S., and Emmenegger, L.: Tracking isotopic
1114 signatures of CO_2 at the high altitude site Jungfraujoch with laser spectroscopy:
1115 analytical improvements and representative results, Atmos. Meas. Tech., 6, 1659-
1116 1671, 2013.
1117 Tarasova, O. A., Brenninkmeijer, C. A. M., Assonov, S. S., Elansky, N. F.,
1118 Röckmann, T., and Brass, M.: Atmospheric CH_4 along the Trans-Siberian railroad
1119 (TROICA) and river Ob: Source identification using stable isotope analysis, Atmos.
1120 Environ., 40, 5617-5628, 2006.
1121 Tuzson, B., Henne, S., Brunner, D., Steinbacher, M., Mohn, J., Buchmann, B.,
1122 and Emmenegger, L.: Continuous isotopic composition measurements of tropospheric

CO2 at Jungfraujoch (3580 m a.s.l.), Switzerland: real-time observation of regional pollution events, Atmos. Chem. Phys., 11, 1685-1696, 2011.

Tuzson, B., Mohn, J., Zeeman, M. J., Werner, R. A., Eugster, W., Zahniser, M. S., Nelson, D. D., McManus, J. B., and Emmenegger, L.: High precision and continuous field measurements of $\delta^{13}C$ and $\delta^{18}O$ in carbon dioxide with a cryogen-free QCLAS, Appl. Phys. B-Lasers and Optics, 92, 451-458, 2008.

Umezawa, T., Aoki, S., Nakazawa, T., and Morimoto, S.: A High-precision Measurement System for Carbon and Hydrogen Isotopic Ratios of Atmospheric Methane and Its Application to Air Samples Collected in the Western Pacific Region, Journal of the Meteorological Society of Japan, 87, 365-379, 2009.

Umezawa, T., Machida, T., Aoki, S., and Nakazawa, T.: Contributions of natural and anthropogenic sources to atmospheric methane variations over western Siberia estimated from its carbon and hydrogen isotopes, Global Biogeochem. Cycles, 26, 2012a.

Umezawa, T., Machida, T., Ishijima, K., Matsueda, H., Sawa, Y., Patra, P. K., Aoki, S., and Nakazawa, T.: Carbon and hydrogen isotopic ratios of atmospheric methane in the upper troposphere over the Western Pacific, Atmos. Chem. Phys., 12, 8095-8113, 2012b.

Vermeulen, A. T., Hensen, A., Popa, M. E., van den Bulk, W. C. M., and Jongejan, P. A. C.: Greenhouse gas observations from Cabauw Tall Tower (1992-2010), Atmos. Meas. Tech., 4, 617-644, 2011.

Wächter, H., Mohn, J., Tuzson, B., Emmenegger, L., and Sigrist, M. W.: Determination of N_2O isotopomers with quantum cascade laser based absorption spectroscopy, Optics Express, 16, 9239-9244, 2008.

WMO: 17th WMO/IAEA Meeting on Carbon Dioxide, Other Greenhouse Gases, and Related Measurement Techniques (GGMT-2013) 10-13 June 2013, GAW Report No. 213,, World Meteorological Organization, Geneva, Switzerland, Beijing, China, 2014.

Wolf, B., Merbold, L., Decock, C., Tuzson, B., Harris, E., Six, J., Emmenegger, L., and Mohn, J.: First on-line isotopic characterization of N_2O above intensively managed grassland, Biogeosciences, 12, 2517-2531, 2015.

Yamada, K., Ozaki, Y., Nakagawa, F., Tanaka, M., and Yoshida, N.: An improved method for measurement of the hydrogen isotope ratio of atmospheric methane and its application to a Japanese urban atmosphere, Atmos. Environ., 37, 1975-1982, 2003.

Zazzeri, G., Lowry, D., Fisher, R. E., France, J. L., Lanoiselle, M., and Nisbet, E. G.: Plume mapping and isotopic characterisation of anthropogenic methane sources, Atmos. Environ., 110, 151-162, 2015.